How the brain adapts to nature's rhythms: a year of neuroimaging in a seasonal mammal

Arsène Ella, Didier Chesneau, Chantal Porte, Didier Lomet, Hans Adriaensen, Benoît Piégu, Ivy Uszynski, Cyril Poupon, Martine Migaud, José Delgadillo, et al.

NeuroImage 321 (2025) 121494

Contents lists available at ScienceDirect

NeuroImage

journal homepage: www.elsevier.com/locate/ynimg

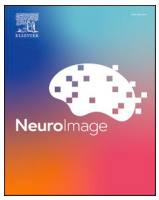

How the brain adapts to nature's rhythms: a year of neuroimaging in a seasonal mammal

Arsène Ella [a], Didier Chesneau [a], Chantal Porte [a], Didier Lomet [a], Hans Adriaensen [a,b], Benoit Piégu [a], Ivy Uszynski [c], Cyril Poupon [c], Martine Migaud [a], José Delgadillo [d], Tiphaine Aguirre-Lavin [e], Olivier Lasserre [e], Philippe Chemineau [a], Hugues Dardente [a], Matthieu Keller [a,*], David André Barrière [a,*]

[a] INRAE, CNRS, Université de Tours, PRC, Nouzilly, F-37380, France
[b] INRAE, Université de Tours, CHU de Tours, PIXANIM, 37380, Nouzilly, France
[c] BAOBAB UMR 9027, NeuroSpin, Université Paris-Saclay, CNRS, CEA, France
[d] CIRCA, Universidad Autonoma Agraria Antonio Narro, Torreon, Mexico
[e] INRAE, UEPAO, Centre de Recherche de Tours, Nouzilly, 37380, France

ARTICLE INFO

Keywords:
Seasons
Brain
MRI
Sheep
Voxel-based morphometry
GM thickness
Brain volume

ABSTRACT

At temperate and polar latitudes, animals and humans experience seasonal changes that impact physiology and behavior. In these habitats, the prevalence and severity of certain psychiatric disorders fluctuate seasonally. Such patterns imply that an adaptive system fine-tunes brain physiology in response to annual environmental changes, and alterations to this system may adversely affect mental health. To date, the core neuronal circuitry of the seasonal control of brain functioning is still largely unknown. To address this question, we identified brain regions sensitive to seasonal changes, using neuroimaging in the domestic sheep (*Ovis aries*), an animal model commonly used to study seasonality. Here, we developed MRI neuroinformatics resources (templates and atlas) dedicated to the analysis of the sheep brain and revealed that seasons broadly modify grey matter organization and volume of both cortical and subcortical regions involved in the control of homeostasis, sensory processing, learning, memory, behavior control, and social cognition. Many of these regions were not previously known to be affected by seasonal variations, highlighting that the seasonal control of brain function involves plasticity mechanisms across multiple brain sites.

1. Introduction

Understanding the physiology of the human brain is the greatest challenge of modern neuroscience and magnetic resonance imaging (MRI) plays a preponderant role in this endeavour. Human neuroimaging research has accelerated over the past decades, fuelled by numerous teams acquiring massive dataset, refining pre-/post-processing and statistical methodologies necessary to achieve the identification of brain territories involved in basic and higher brain functions in health and disease (Grandjean et al., 2023; Mandino et al., 2020). Despite intense research, we still know little about brain diseases and many of these, including psychiatric conditions, may not benefit from fully appropriate treatments and therapies as we ignore their inner roots (Homberg et al., 2021). In this context, experimental neuroscience using animal models is critical to gain insights into brain functioning. Nevertheless, preclinical MR-imaging in animals lags far behind humans

Abbreviations: ANTs, advanced normalization tools; BIDS, brain imaging data structure; CNR, contrast-to-noise ratio; CSF, cerebrospinal fluid; CT, computed tomography; DARTEL, diffeomorphic anatomical registration through exponentiated lie algebra; FBER, foreground to background energy; FOV, field of view; FSL, FMRIB software library; FWHM, full width at half maximum; GHT, geniculohypothalamic tract; GMC, grey matter concentration; GM, grey matter; GnRH, gonadotropin-releasing hormone; MEDIC, multiple echo data image combination; MRI, magnetic resonance imaging; MPRAGE, magnetization prepared rapid gradient echo; PT, *pars tuberalis*; RIA, RadioImmunoAssay; ROI, region of interest; SCN, suprachiasmatic nucleus; SNR, signal-to-noise ratio; SPC-IR, short tau inversion recovery; SPM, statistical parametric mapping; T1, T1-weighted imaging; T2*, T2*-weighted imaging; TE, echo time; T3, triiodothyronine; TR, repetition time; TSH, thyroid-stimulating hormone; VBM, voxel-based morphometry; WM, white matter.

* Corresponding authors.
E-mail addresses: matthieu.keller@inrae.fr (M. Keller), david.barriere@cnrs.fr (D.A. Barrière).

https://doi.org/10.1016/j.neuroimage.2025.121494
Received 13 May 2025; Received in revised form 16 September 2025; Accepted 29 September 2025
Available online 30 September 2025

imaging. In basic neuroscience, most studies involve rodents and specific methodological developments (high fields magnet, cryo-coils etc.) had to be unlocked to ensure data quality and repeatability of MRI measurements. Additionally, the creation of standard spaces (templates) and brain atlases necessary to achieve group studies were limited until recently (Barrière et al., 2021, 2019; Kleven et al., 2023; Wang et al., 2020). These methodological issues must be addressed before the scientific community can adopt a unified approach, ensuring better repeatability and more efficient comparisons between datasets. For instance, the development and validation of a benchmark procedure for functional MRI data acquisition and analysis dedicated to the rat brain was achieved in 2023, which provides solid guidelines for improved studies in this rodent species (Desrosiers-Grégoire et al., 2024; Grandjean et al., 2023; Vrooman et al., 2025).

However, all questions cannot be addressed with the sole rodent models and other species such as hamsters, guinea pig, sheep, and non-human primates are invaluable models, which offer specific physiological or behavioural traits that make them more valid models than rodents to address specific fundamental or disease-related questions. As an example, within the field of psychiatry, seasonal variations of brain functioning is an emergent and salient question (Zhang et al., 2023). Indeed, in high-latitude territories, where seasonal variations of photoperiod are marked, the prevalence of mood disorders significantly increases (seasonal affective disorders, suicide, etc.) (Bauer et al., 2019; Kegel et al., 2009; Kinney et al., 2009; Patten et al., 2017; Rosen et al., 1990). Additionally, post-mortem, SPECT/PET and MR imaging showed that seasons dynamically regulate the homeostasis of both dopaminergic and serotonergic systems (Zhang and Volkow, 2023), glucose metabolism in prefrontal regions, cuneus, brainstem, postcentral cortex and olfactory bulb and functional connectivity in healthy humans brain (Xu et al., 2023). In line with those results, some studies demonstrated seasonal variations of cognitive performances for sustained attention and working memory task suggesting that seasonal variations of brain homeostasis is associated with cognition and memory (Meyer et al., 2016). Taken together, current data suggest that humans are sensitive to photoperiodic variations, which validates the persistence of an adaptative system for tuning brain physiology and individual behavior along the year. Misalignment of this inner system with environmental cues may elicit negative consequences on mental health.

To understand how seasons shape brain structure and function over the year, the use of a seasonal animal model is required. The sheep (*Ovis aries*) displays an array of physiological functions that are seasonally regulated by photoperiod and is a classical model to study seasonality of brain functions (Dardente, 2015; Dardente et al., 2019). Seasonal functions are regulated by a circannual clock located within the pituitary *pars tuberalis* (PT), which is daily entrained by the fluctuations of nightly pineal release of melatonin. The duration of melatonin secretion is tightly correlated with night duration and acts as a neuroendocrine index encoding photoperiod (Dardente et al., 2019). This neuroendocrine index is integrated by PT-located thyrotroph cells which produce thyroid-stimulating hormone (TSH) exclusively under long spring/-summer days (Dardente et al., 2014). TSH then acts retrogradely on specific ependymal cells, known as tanycytes, through its cognate receptor to control local hypothalamic levels of thyroid hormone. This mechanism ensures heightened production of bioactive triiodothyronine (T3) as day length increases, which then impacts the microstructural organization of the hypothalamus (Migaud et al., 2015, 2011) and the activity of specific neuronal populations to control breeding/lactation, social/feeding behaviors, as well as metabolism (Hazlerigg and Simonneaux, 2015). Nevertheless, if the cellular and molecular mechanisms responsible for the integration of seasonal cues within the hypothalamus are well-known and detailed, the effect of the seasons on structures involved in cognition and/or memory have never been investigated in sheep.

To address this question, we developed a comprehensive neuroimaging resource, the Turone Sheep Brain Template and Atlas, dedicated to the analysis of ovine brain MRI data. Given that seasonality involves tissue reorganization, at least in the hypothalamus, we used these tools to conduct a longitudinal MRI morphometric study using voxel-based morphometry (VBM). VBM is a well-established and validated image analysis technique capable of detecting subtle changes in brain parenchyma features, such as cell size, neurogenesis, apoptosis, spine density, and vasculature, in both animals and humans (Keifer et al., 2015; Lerch et al., 2011; Streitbürger et al., 2012). In addition, we examined both grey matter (GM) thickness and the regional volumes of key structures (e.g., hippocampus, amygdala, etc.) to elucidate the dynamics of seasonal brain structural modifications. Our findings reveal the surprisingly extensive and complex reorganization that seasons induce across multiple brain regions, which may collectively influence a broad spectrum of brain functions in seasonal mammals.

2. Material and methods

2.1. Animals

Seventeen adult, sexually mature multiparous ewes (*Ovis aries*), aged 3.4 ± 0.3 years and weighing 64.5 ± 5.5 kg, were included in this study and scanned at the PIXANIM facility (INRAE, French National Research Institute for Agriculture, Food & Environment, Nouzilly, France). Ewes were ovariectomized and implanted subcutaneously with a 2 cm silastic implant containing 100±15 mg 17β-estradiol at the end of October, two months before the first scan session. The ewes were kept permanently indoors and fed ad libitum with dehydrated lucerne, maize, straw, and a supplement of vitamins and minerals and had free access to water. All procedures were conducted in accordance with the European directive 2010/63/EU on the protection of animals used for scientific purposes, and the experimental protocol was approved by the local ethical committee for animal experimentation (CEEA VdL, Tours, France, ref. 00.510.02).

2.2. Surgical procedure

Ewes were fasted for 24 h before surgery. On the day of surgery, an intravenous injection of thiopental (14 mg/kg body weight; Nesdonal, Merial, France) was administered to induce analgesia. Animals were then intubated and maintained under anaesthesia with a mixture of 3–4 % isoflurane (Vetflurane, Virbac, France) vaporized in 100 % oxygen. The ovariectomy was performed under sterile surgical conditions. Local anaesthesia with lidocaine (4 %, Lurocaïne, Vétoquinol, France) was administered prior to laparotomy to relieve pain. The ovaries were surgically removed, the silastic 17β-estradiol implant was placed and the tissues were sutured. This model normalizes the level of circulating 17β-estradiol, which uncovers the well-documented central seasonal shift in the negative feedback action of 17β-estradiol on gonadotropin secretion (Karsch et al., 1984; Legan et al., 1977) and facilitates interpretation as ovariectomy excludes the potential implication of other ovarian steroids (e.g. progesterone) in the observed changes. Postoperative ventilation with oxygen was maintained until the first signs of awakening appeared. The animals were then housed individually for 6 h in a padded stall before being returned to their congeners. They received an anti-inflammatory drug for 2 days (2 mg/kg flunixin meglumine, Finadyne®, Intervet, France) to relieve pain and an anti-oedema medication (1 mg/kg furosemide, Dimazon®, Intervet, France) at the end of the surgery. Finally, the animals were treated with a diuretic medication combining 3 mg/kg of hydrochlorothiazide with 0.03 mg/kg of dexamethasone (Diurizone®, Vétoquinol, France) for 2 days.

2.3. Photoperiodic conditions

Two scanning sessions were conducted for each animal at opposite times of the annual cycle. The first session took place from January 13, 2014, to February 17, 2014, marking the end of the breeding season for

intact animals. The second session was conducted between June 16, 2014, and July 22, 2014, corresponding to the end of the sexual rest season for intact ewes. As 4–5 weeks were required to scan the entire group, the animals were brought indoors for two weeks before and during each scan session and kept under controlled photoperiodic conditions. This ensured that each subject experienced a similar light duration and avoided any photoperiodic shift over the scanning sessions. The winter scanning session had a mean daylight of 556.1 ± 22.26 min, while the summer scanning session had a daylight duration of 943.3 ± 13.90 min. Therefore, during the winter scan session, ewes were housed under a 16-h dark/8-h light cycle, and during the summer scan session, they were under an 8-h dark/16-h light cycle (Fig. S1). Between both sessions animals were housed under natural light conditions in open barns.

2.4. Melatonin response to photoperiodic exposure

To ensure that the animals were responsive to the photoperiodic treatment, serial blood samplings were performed overnight to assay melatonin in blood plasma one week before the start of each MRI scan session. Briefly, animals were housed individually for 24 h and implanted with a catheter into the jugular vein before blood sampling to minimize any potential stress response. Blood sampling was performed under dim red-light hourly, starting one hour before the lights were turned off and pursued until two hours after lights were turned on. The blood samples were then centrifuged, and the plasma was stored at −80 °C until the assay. Melatonin was assayed by a direct RIA method described previously (Zarazaga et al., 2010) with 2-[125I] iodomelatonin as a tracer (Vakkuri et al., 1984) and a previously described anti-melatonin antiserum (Tillet et al., 1986). This direct assay, originally described by Fraser et al. (1983), was performed according to the modifications of Webley and Luck (1986) and Ravault et al. (1989). Briefly, 100 µl rabbit anti-melatonin antiserum (final dilution: 1/400 000) and 300 µl 2-[125I] iodomelatonin (15.000 c.p.m./tube) were added to 100 µl assay buffer (tricine) or undiluted plasma. After 16–18 h of incubation at 4 °C, the antigen–antibody complexes were precipitated by addition of 1 ml sheep anti-rabbit antiserum (INRA). After one hour of incubation, the samples were centrifuged (2800 g for 30 min at 4 °C), then the supernatant was discarded and the pellet counted on a Gamma counter. (Fig. S1).

2.5. In vivo MRI acquisitions

Animal preparation for MRI data acquisitions was performed as previously described (Ella et al., 2017; Ella and Keller, 2015). Briefly, animals were anesthetized with an intramuscular injection of ketamine just before the scan, intubated, maintained during the scan on 3 % isoflurane vaporized in oxygen, and continuously monitored by an MR-compatible Aestiva®/5 system (Madison, USA). Three MR acquisitions were performed (see Ella and Keller, 2015 for details) on each animal, secured in a prone position in a 3T VERIO Siemens system (Erlangen, Germany), with front legs apart and bent towards the abdomen, using a flexible coil (Siemens FLEX Large 4 elements) tied around the head. The sequences have been optimized in order (*i*) to be acquired within a timeframe compatible with the duration of anaesthesia (≤1 h), (*ii*) to reduce artifacts (folding, truncation, etc.), and (*iii*) to optimize SNR. For each acquisition, parameters have been set as previously described in Ella and Keller (2015):

- Three-dimensional SPC-IR acquired in sagittal plane (Echo Time/Repetition Time = 413 ms/4000 ms, Flip Angle = 120°, Inversion Time = 380 ms, Number of Excitation = 10, Partial Fourier = 1, Slice Thickness = 0.35 mm, Slice Number = 208, Field of View = 179.2 × 179.2 mm, matrix = 512 × 512, final resolution 0.35 mm^3).
- Three-dimensional T_1 MPRAGE acquired in sagittal plane (Echo Time/Repetition Time = 3.18 ms/2500 ms, Flip Angle = 12°, Inversion Time = 900 ms, Number of Excitation = 8, Partial Fourier = 1, Slice Thickness = 0.5 mm, Slice Number = 288, Field of View = 192 × 192 mm, matrix = 384 × 384, final resolution 0.5 mm^3).
- Three-dimensional T2* MEDIC acquired in sagittal plane (Echo Time/Repetition Time = 2.1 ms/38 ms, Flip Angle = 8°, Number of Excitation = 6, Partial Fourier = 0.75, Slice Thickness = 0.4 mm, Slice Number = 256, Field of View = 179.2 × 179.2 mm, matrix = 448 × 448, final resolution 0.4 mm^3).

At the end of the acquisitions, animals were transferred from the scanner to a recovery room, anaesthesia was stopped, and mechanical ventilation was maintained. As soon as the first signs of awakening were noticed, animals were extubated and placed under constant surveillance in a dedicated pen. When fully awake, the animal was returned to the indoor facilities with its conspecifics until the end of the data acquisition session. DICOM data from the scanner were converted to NIFTI format and organized as standardized datasets according to the Brain Imaging Data Structure (BIDS) using BIDScoin. Raw MRI data collected during this experiment can be downloaded from Zenodo.

2.6. TSBTA environment updating

2.6.1. Version 1 of Turone sheep brain template and atlas

The first version of the TSBTA was created from 18 scans of ovariectomized Ile-de-France ewes (3.4 years old), which had been implanted with a 17β-estradiol silastic implant (2 cm) at least two months before the scan session. Similar MRI acquisitions were performed, and a multimodality template (T_1 and T_{2*}) was created using linear and nonlinear normalization procedures scripted with the FSL5.0 software library (FMRIB, University of Oxford, UK). Additionally, three prior probability maps (grey matter = GM, white matter = WM, and cerebrospinal fluid = CSF) were generated using FSL-FAST for automatic segmentation of the ovine brain (Ella and Keller, 2015). Finally, an atlas of the entire brain was created by delineating twenty-five cortical gyri and twenty-eight inner sheep brain structures within the cerebrum (Ella et al., 2017). From this previous environment, both the templates and prior probability maps were updated using cutting-edge methods proposed by the ANTs environment. Indeed, the accuracy and specificity of the probabilistic maps (GM, WM, CSF) had the potential to be improved. Additionally, within the first version of the brain atlas, the thalamic region was not fully segmented, and this gap had to be filled.

2.6.2. Updating of MRI templates and probabilistic maps

Before post-processing steps, SPC-IR, T_2 MEDIC and T_1 MPRAGE images acquired for each animal (34 scans by contrast) were noise- and signal-bias corrected using Ginkgo and N4BiasFieldCorrection respectively and coregistered to the first version of the TSBTA using antsRegistrationSyNQuick. Hence, both SPC-IR and T_2 MEDIC images were resampled to a voxel size of 0.5 mm^3. Together, all coregistered data (T_1, IR, T_{2*}) were used to segment each brain using antsAtroposN4 to create GM, WM and CSF probabilistic maps for each subject. In parallel, we used modelbuild, an optimized pipeline using antsMultivariateTemplateConstruction2, an unbiased template building method developed in ANTs package. This method has been integrated to our local cluster (ISLANDe Facilities) and require qbatch and slurn. For computation, our cluster comprises 240 physical cores, each associated with 9.6GB of memory (2.3 TB of memory in total), with 90 TB of long-term storage and 72 TB of high-performance storage. Once both linear and non-linear (flow-field) maps were calculated for each animal, we compiled all transformations calculated for each image and applied them once to denoised and signal bias corrected images (SPC-IR, T_2 MEDIC and T_1 MPRAGE) using antsApplyTransforms to limit interpolation effects. SPC-IR, T_2 MEDIC and T_1 MPRAGE images have been used to create the second version of the TSBTA templates by calculating the mean image of each normalized contrast using Ginkgo. Probabilistic maps (GM, WM, CSF) from each subject have been normalized using antsApplyTra

nsforms by applying both linear and non-linear transformation provided by modelbuild. The second version of the GM, WM and CSF priors of the TSBTA were built by calculating the mean image of each normalized map using Ginkgo.

2.6.3. Atlas updating

The first version of the TSBTA T_1 template has been linearly and non-linearly coregistered to the second version TSBTA T_1 template using antsRegistrationSyNQuick and both linear and non-linear transformations have been applied to the first version of the TSBTA atlas using antsApplyTransforms to create the second version of the TSBTA atlas (Fig. S2). Each region of interest (ROI) was visually inspected to check the boundaries and accuracy of the registration. Some ROIs, such as the *corpus callosum, arbor vitae*, and ventricular systems, were updated using WM and CSF priors for the best fit to the new version of the templates. Eventually, the thalamus was fully segmented manually using the fsleyes and itksnap platforms, and the ROIs were labelled according to the work previously published in humans (Iglesias et al., 2018).

2.6.4. Additional feature: computed tomography (CT) sheep template

Tomographic data for the skulls of nine ewes were acquired using our CT scanner (Siemens Somatom Definition AS, Siemens Corp., Germany). The X-ray source was set at 100 kV and 120 mA/s. A total of 800 slices were acquired with the following parameters: thickness = 0.4 mm, slice number = 800, field of view = 204.8 × 204.8 mm, matrix = 512 × 512, and final resolution = 0.4 mm^3, reconstructed using a Safire I26 filter. DICOM data were converted to NIfTI format and organized as standardized datasets using BIDScoin. Data can be downloaded from Zenodo. To create a CT template from our data, we first performed a linear coregistration of all the data to the first animal using antsRegistrationSyNQuick. Then we used modelbuild, to create both linear and non-linear transformations for each animal. All the transformations calculated previously were compiled and applied once to raw CT images using antsApplyTransforms to limit interpolation effects. Spatially, normalized CT images were used to create a temporary version CT template by calculating the mean image of the normalized dataset using Ginkgo. Finally, the CT template was coregistered to the second version of the Turone T_1 template manually using the Anatomist tool of the BrainVISA suite and resampled at the same spatial resolution (0.5 mm^3). The manually coregistered CT template was then linearly and non-linearly coregistered to the second version of the Turone T_1 template antsRegistrationSyNQuick. Eventually, all the transformations calculated from raw up to this point were compiled and applied once to raw CT images using antsApplyTransforms and the final version CT template was created by calculating the mean image of the normalized dataset using Ginkgo (Fig. S3).

2.7. Voxel-based morphometry and GM thickness data analysis

For voxel-based morphometry analysis (VBM), we utilized the T_1 MPRAGE images (T_1), which have the highest contrast-to-noise ratio in our dataset and were acquired at the same resolution as the second version of the TSBTA T_1 template. For each animal ($n = 17$), two images are available (Winter and Summer). The data were first denoised and corrected for signal bias using Ginkgo and N4BiasFieldCorrection respectively and linearly coregistered to the TSBTA T_1 template using antsRegistrationSyNQuick. The coregistered data were then pre-processed with SPM. Each image was segmented into probability maps of GM, WM and CSF using the default settings in the SPM8 toolbox and the new version of GM, WM, and CSF probability maps. The transformation matrices obtained were used to normalize the GM, WM, and CSF probability maps for each subject. Both GM and WM probability maps of each scanning session were normalized to our stereotaxic space using the transformation matrices obtained and resampled. Normalized GM and WM images were used to create a more population-specific template using diffeomorphic anatomical registration through exponentiated Lie algebra (DARTEL) (Ashburner, 2007; Ashburner and Friston, 2005, 2000). Each normalized GM image was then warped using deformation parameters calculated by the DARTEL routine of SPM and modulated to correct for volume changes that may have occurred during the deformation step. Finally, the normalized-warped-modulated GM images were spatially smoothed by convolving with a 4 mm full width at half-maximum (FWHM) isotropic Gaussian kernel to create grey matter concentration (GMC) maps (Fig. S4).

GM thickness was computed using the DiReCT algorithm (Diffeomorphic registration-based GM thickness) from the ANTs package (ants.kelly_kapowski) which estimates the GM thickness by analysing the distance between the GM/WM boundary and the GM/CSF boundary. Here, the previously calculated GM, WM and CSF probability maps were used to feed the ants.kelly_kapowski function, which assigned at each spatial location within the cortex the distance between the GM boundaries. A more detailed explanation of this ANTs function has been published by Das et al. (2009). Then GM thickness maps were normalized to the template space using the previous procedure and were spatially smoothed by convolving with a 4 mm FWHM filter.

2.8. Voxel-based morphometry and GM thickness statistical analysis

To assess regional grey matter and GM thickness changes between the two seasons across all animals, GMC and GM thickness maps obtained during the winter period were compared to those obtained during the summer period for each animal using a paired *t*-test proposed by SPM. A brain mask was used to constrain the analysis to the brain and brain volume of each animal has been used as a regressor. For each cluster, the significance of the peak voxel was set at $p < 0.005$ (t-score = 2.92, degree of freedom = 16). The results are presented on brain slice series generated with Nilearn.

2.9. Volumetric data analysis

Eventually, inverse spatial transformations data from every subject and session were applied to the Turone Sheep Brain Atlas using antsRegistrationSyNQuick, to map them onto each subject/session's native brain spaces. Then, the volume of each individually mapped ROI was calculated (in cubic millimetres) and then compiled into a structured CSV file. From this data, the mean volume difference (in mm^3) between summer and winter sessions for each brain ROI (Table S2) and significant seasonal modifications ($p < 0.05$) were identified using a linear regression model with fixed effects for subject, session and brain volumes (Table S1), followed by a permutation test (10.000 permutations).

2.10. Post-processing statistical analysis

Significant clusters from the VBM and GM thickness analysis revealed by SPM, were identified using our atlas and a specific procedure developed in MATLAB. For each comparison, ROI masks from the second version of the TSBTA atlas were used to extract both GMC and GM thickness values of corresponding regions within corresponding maps using the REX plugin. Group comparisons (Winter *versus* Summer) of GMC and GM thickness data were compiled and analysed using GraphPad Prism 10.2.0 software, and were compared using a Wilcoxon matched-pairs signed rank test using False Discovery Rate (FDR) for multiple comparisons and the two-stage step-up (Benjamini, Krieger and Yakutieli) method for a desired FDR (Q) value = 1 % (*** $p < 0.001$)

3. Results

3.1. Turone sheep brain template and atlas updating

The VBM strategy requires a brain template space and its associated priors of GM, WM and CSF for brain tissue segmentation and spatial

normalization. Additionally, a complete atlas of the sheep brain in the same space is essential for identifying ROIs highlighted by the VBM analysis. Given the limitations of the available tools to thoroughly study GMC changes induced by photoperiod, we first updated the resources we had previously developed in sheep.

3.1.1. Template updating

Compared to our previous FSL-built T_1 template, the second version of the TSBTA was constructed using methods developed by the ANTs package and data acquired with the same MRI sequences. Visual inspection clearly shows that the T_1 templates of this second version are much less blurred and exhibit improved contrast (Fig. 1a). Some previously undetermined structures, such as the *fimbria* of the hippocampus (Fig. 1a, red arrows), are now clearly defined. Additionally, we visually improved brain segmentation using the multimodal approach offered by the ANTs toolkit. Compared to the previous priors, the GM, WM, and CSF maps are less blurred in this second version. Some areas have shifted from the GM to the WM compartment, such as the pituitary gland (Fig. 1a, green arrows, and Fig. 1c), or from GM or WM to CSF (Fig. 1a, blue arrows). To objectively evaluate the improvement of our data, quality metrics have been calculated on each template image:

- Signal-to-Noise Ratio (SNR): The mean intensity within the GM divided by the standard deviation of the values outside the brain. Higher values indicate better quality (Magnotta and Friedman, 2006).
- Contrast-to-Noise Ratio (CNR): The mean of the GM intensity values minus the mean of the WM intensity values, divided by the standard deviation of the values outside the brain. Higher values indicate better quality (Magnotta and Friedman, 2006).
- Foreground to Background Energy Ratio (FBER): The variance of voxels inside the brain divided by the variance of voxels outside the brain. Higher values indicate better quality (Huang et al., 2016).

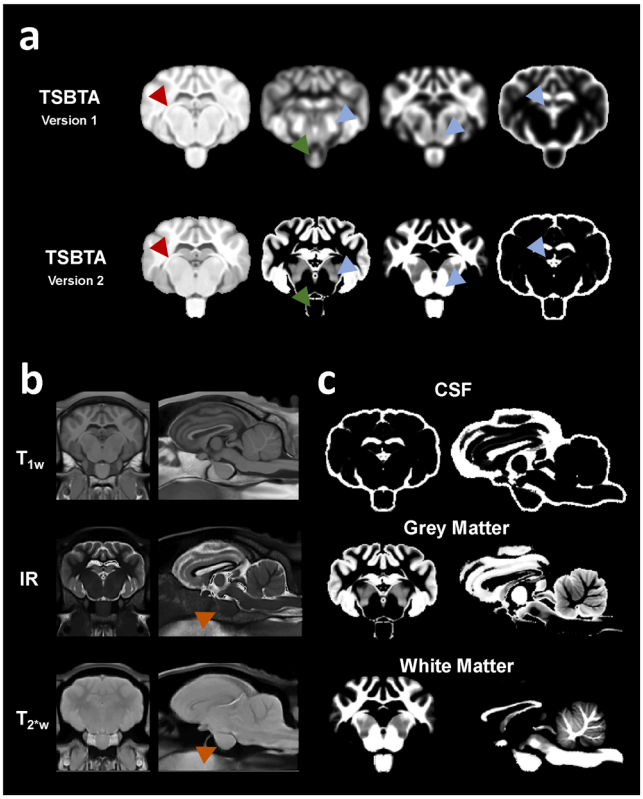

Fig. 1. Updating of the TSBTA templates and tissue probability maps. (a) Coronal views of the first (top) and second (down) anatomical T_1 template of sheep brain at the same coordinates. (b) Coronal and sagittal views of three contrasts (T_1 MPRAGE, SPC-IR and T_2* MEDIC) available with the second version of TSBTA. (c) Coronal and sagittal view of cerebrospinal fluid (CSF), grey matter and white matter probability maps of the second version of TSBTA at the same coordinates.

As shown in Table 1, the second version of the T_1 sheep brain template displays higher quality metrics compared to the first version. The second version shows a 26.74 % improvement in SNR (from 5.25 to 6.65), a 71.71 % improvement in CNR (from 0.95 to 1.63), and a 95.63 % improvement in FBER (from 0.52 to 1.02). These results demonstrate that the quality of the T_1 template has been significantly improved in the second version of the TSBTA. Moreover, the SPC-IR modality (IR Template) is the most contrasted template, with higher quality metrics compared to the T_1 template: SNR is 14.07 (112 % higher), CNR is 7.75 (375 % higher), and FBER is 35.18 (3350 % higher). Finally, the T_{2^*} template provided in the second version of the TSBTA is the least contrasted template, with lower quality metrics compared to the T_1 template: SNR is 5.90 (11 % lower), CNR is 0.29 (82 % lower), and FBER is 0.44 (57 % lower). Nevertheless, the T_{2^*} template is still the most specific template, as a homogeneous signal is observed in all brain parenchyma as well as in the pituitary and spinal cord regions (Fig. 1b, orange arrows).

3.1.2. Stereotaxic reference coordinates and atlas updating

A brain atlas serves as a detailed map that facilitates the identification of brain regions involved in biological or pathological processes and aids in navigating the brain to reach a specific target. To identify a region or a target point, a stereotaxic reference system is essential. In the second version of the TSBTA, we used CT scans that were spatially normalized to the T_1 MRI template (Fig. 2a) to define a stereotaxic reference for the ovine brain. For this purpose, we selected the lambda point of the skull, defined as the intersection between the sagittal and lambdoid sutures of the skull bones, for the following reasons:

- It is easily recognizable on both CT and MRI scans, as well as on the surface of the skull during surgery.
- It is precisely located above the interhemispheric sulcus, effectively dividing the brain into left and right hemispheres.
- The distance between the theoretical location of the lambda in the TSBTA CT space and its actual location after rigid co-registration of individual CT data is minimal (left-right axis: ±0.33 mm, rostrocaudal axis: ±2.93 mm, dorsoventral axis: ±0.99 mm, Figs. 2b and S5).

This means that using a stereotaxic device to position animals similarly to the TSBTA space allows for feasible brain navigation with a reduced risk of error. In this standardized and referenced space, we normalized the first version of the TSBTA atlas (Fig. S2). The original TSBTA atlas consisted of a mosaic of 106 ROI, including 25 cortical and 28 subcortical regions, bilaterally. In the second version, we retained the

Table 1
Estimation of the quality of the TSBTA between version and modality.

Modality	TSBTA Version 1	TSBTA Version 2		
	T1	T1	IR	T2*
SNR	5.2467	6.6495	14.0727	5.9033
CNR	0.9482	1.6282	−7.7479	−0.2874
FBER	0.5214	1.0200	35.1825	0.4383
EFC	−1.8204e+04	−1.4360e+04	−1.3215e+04	−1.3907e+04

Using SPMUP toolbox we computed between the Grey Matter (GM) and the White Matter (WM) of two version of the TSBTA and between the three-modality available in the second version of the TSBTA the SNR (Signal-to-Noise Ratio), CNR (Contrast-to-Noise Ratio) and FBER (Foreground to Background Energy Ratio) as criterion to estimate the quality of the different templates proposed.

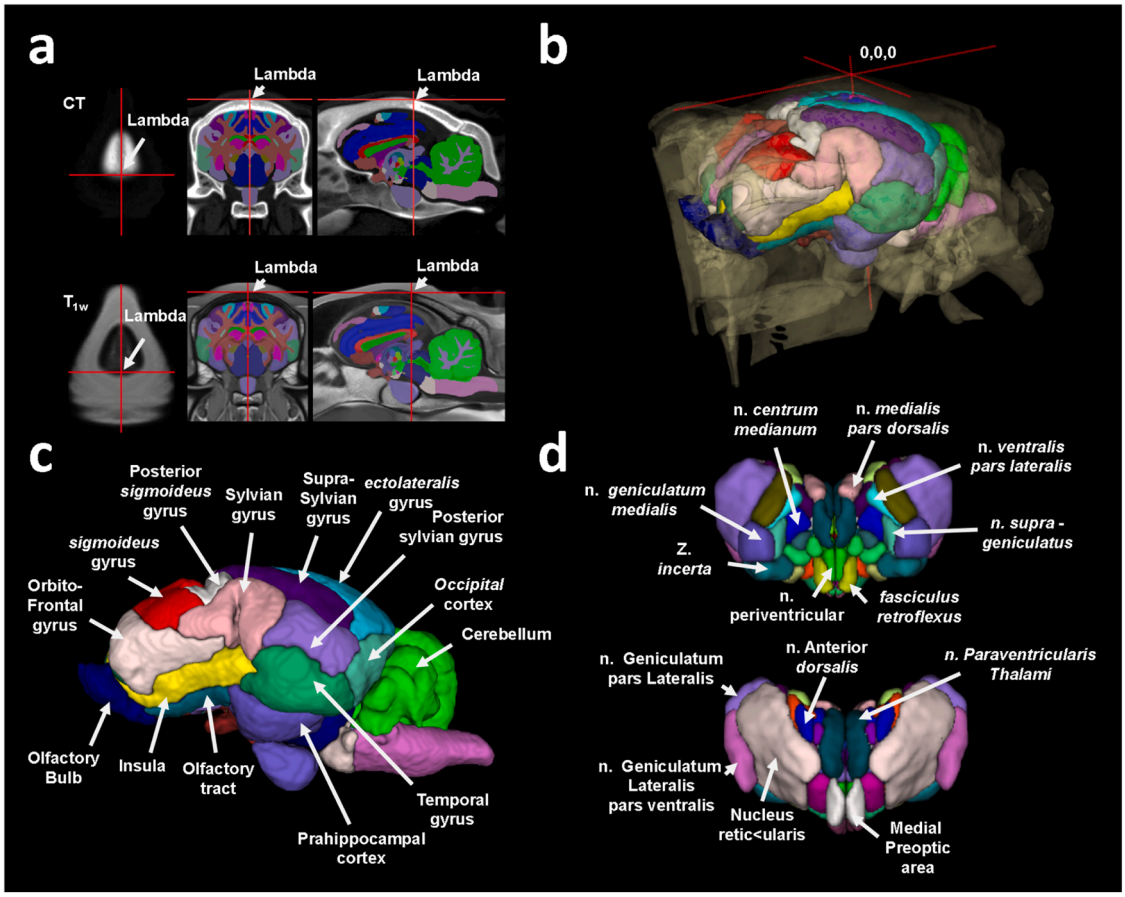

Fig. 2. Updating of the TSBTA atlas and TSBTA CT skull template. (a) Axial, coronal, and sagittal view CT template. Cross hairs showing the position of the lambdoid suture which is used as reference point within the TSBTA space. (b) 3D representation of the TSBTA space. Yellow shaded mesh represents the skull and crosshair represent the reference point of the skull (lambdoid suture position). (c) Sagittal view of TSBTA brain atlas. (d) Anterior (top) and posterior (down) 3D view of the thalamus segmentation.

original segmentation (Fig. 2c) and further added a complete segmentation of the thalamus (Fig. 2d), which plays many pivotal roles in both animal and human physiology. We segmented the thalamus into 102 regions (51 per hemisphere), allowing for the identification of numerous nuclei, such as the lateral and ventral geniculate nuclei, which are critical relays of the geniculohypothalamic tract (GHT). We also segmented additional extra-thalamic regions (e.g., the medial preoptic area) and extra-cephalic regions, such as the skull, frontal sinus, internal auditory meatus, ethmoidal labyrinth, and soft tissue regions, based on the boundaries of the CT template. Overall, our final sheep brain atlas comprises a mosaic of 208 ROI and could be used to create a standardized 3D sheep brain diagram like those available for rodents and humans (Fig. 3).

3.2. *Seasonal modifications in microstructural grey matter*

Next, we used our new resources to assess potential variations in GMC in sheep brains exposed to either winter or summer photoperiods. Using MRI T_1 anatomical acquisitions, we estimated the GMC maps, which offer a global estimation of brain GMC for each animal. A comparison of GMC maps from 17 animals, analysed first in January/February and then again in June/July, demonstrated significant modifications in GMC between the two periods for several nuclei/regions (Fig. 4). GMC values were higher in summer than in winter in the pineal gland (orange color; winter = 0.5216 ± 0.02778; summer = 0.5352 ± 0.02573, p-value = 0.0016, Fig. 5a) and within the medio-basal hypothalamus (winter = 0.2908 ± 0.014454; summer = 0.2983 ± 0.01324, p-value < 0.001, Fig. 5b). In contrast, a significant decrease in GMC (indicated in blue in Fig. 4) was observed within the supragenicular nucleus (winter = 0.1437 ± 0.01538; summer = 0.1358 ± 0.01212, p-value < 0.001, Fig. 5c). Significant increases in GMC were also found in several cortical territories, such as the occipital gyrus (winter = 0.6652 ± 0.01317; summer = 0.6729 ± 0.01334, p-value < 0.001, Fig. 6a), the temporal gyrus (winter = 0.7007 ± 0.01012; summer = 0.7071 ± 0.01018, p-value < 0.001, Fig. 6b), the parahippocampal cortex (winter = 0.678 ± 0.01682; summer = 0.6859 ± 0.01611, p-value < 0.001, Fig. 6c), the claustrocortex (insula) (winter = 0.7713 ± 0.01313; summer = 0.7819 ± 0.01343, p-value < 0.001, Fig. 6d), the rectus gyrus (winter = 0.7166 ± 0.00884; summer = 0.7713 ± 0.01313, p-value < 0.001, Fig. 6e), and the cingulate cortex (winter = 0.8016 ± 0.01353; summer = 0.8083 ± 0.01212, p-value < 0.001, Fig. 6f). Finally, the increase in day length induced a significant increase in GMC in subcortical regions such as the amygdala (winter = 0.7664 ± 0.00719; summer = 0.7701 ± 0.00712, p-value < 0.001, Fig. 7a), hippocampus (winter = 0.7511 ± 0.01237; summer = 0.7575 ± 0.01217, p-value < 0.001, Fig. 7b), habenular nucleus (winter = 0.5429 ± 0.02642; summer = 0.5538 ± 0.02451, p-value < 0.001, Fig. 7c), septum (winter = 0.6351 ± 0.01057; summer = 0.6450 ± 0.0113, p-value < 0.001, Fig. 7d), and the olfactory bulb (winter = 0.4819 ± 0.01288; summer = 0.4975 ± 0.01414, p-value < 0.001, Fig. 7e). Finally, GMC exhibited lower values within the periaqueductal grey in summer compared to winter (winter = 0.2808 ± 0.01624; summer = 0.2709 ± 0.01594, p-value < 0.001, Fig. 7f).

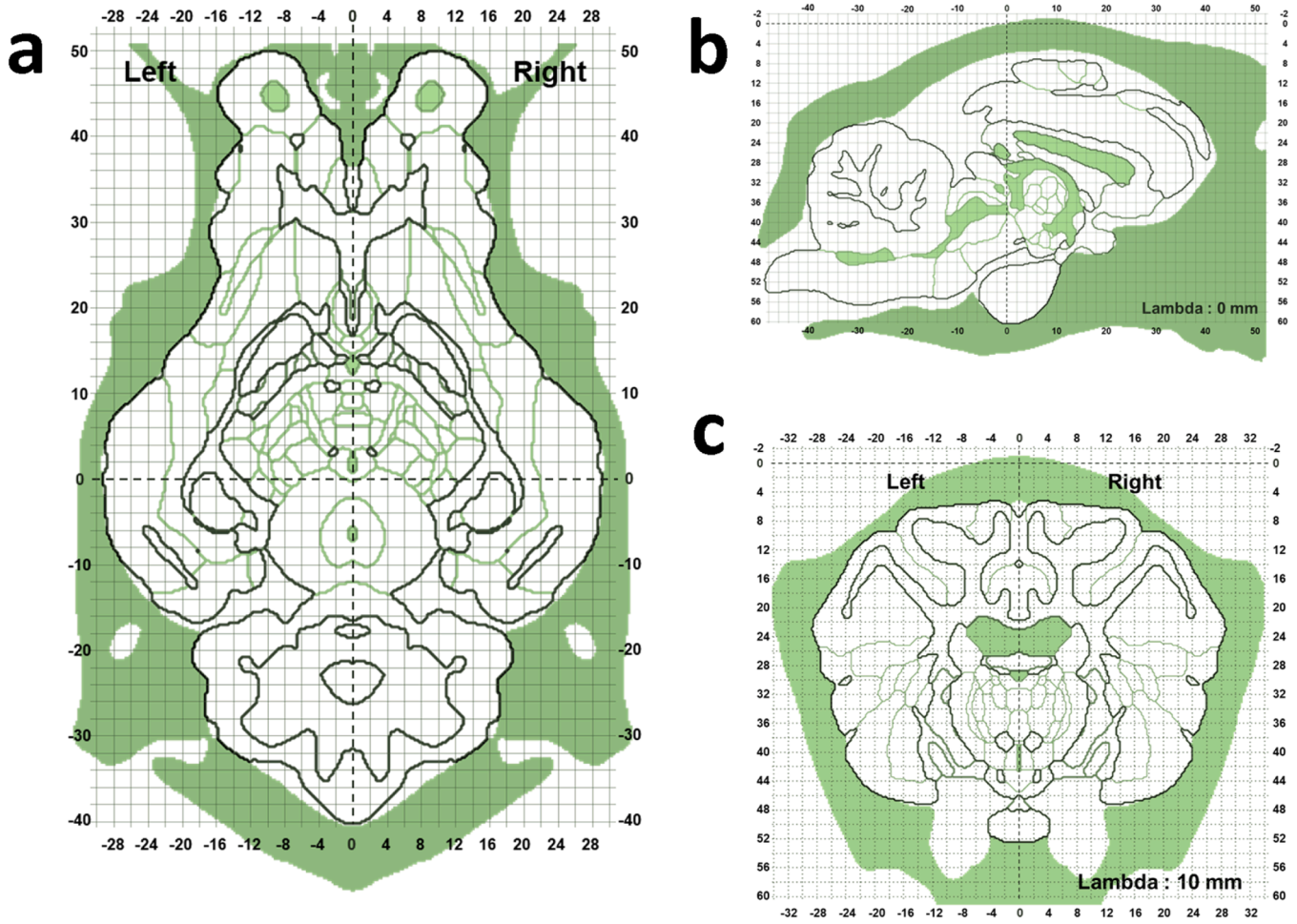

Fig. 3. Two-dimensional representation of the Turone sheep brain atlas in stereotaxic coordinates. Coronal (a) Sagittal (b) and axial (c) slices.

3.3. *Seasonal modifications of GM thickness and volumes*

GMCs modifications could be interpreted as alterations in cell size, proportion of neural or glial cells, cell division or apoptosis, changes in spine density, or modifications in blood flow (Keifer et al., 2015; Lerch et al., 2011; Streitbürger et al., 2012). Thus, the GMC index is known to mix numerous kinds of cellular modifications, and it should be completed by additional metrics to properly assess brain anatomical modifications over the seasons. To explore this further, we evaluated the effect of the seasons on GM thickness, a more easy-to-read index which we found significantly modified within 41 brain regions (Table S3 and Fig. 8). Notably, that GM thickness was significantly lower (indicated in blue in Fig. 8) in summer when compared to winter within the precruciate (winter = 2.885 mm ± 0.345; summer = 2.699 mm ± 0.352, p-value < 0.001, Fig. 9a) and postcruciate gyrus (winter = 1.920 mm ± 0.336; summer = 1.762 mm ± 0.278, p-value < 0.001, Fig. 9b), within the insula (winter = 2.321 mm ± 0.327; summer = 2.166 mm ± 0.306, p-value < 0.001, Fig. 9c) and the striatum (winter = 1.075 mm ± 0.121; summer = 0.948 mm ± 0.118, p-value < 0.001, Fig. 9d). GM thickness was higher in summer than in winter (indicated in orange in Fig. 8) within the right parahippocampal cortex (winter = 0.5216 ± 0.02778; summer = 0.5352 ± 0.02573, p-value = 0.0016, Fig. 9e) and within the right temporal gyrus (winter = 0.2908 ± 0.014454; summer = 0.2983 ± 0.01324, p-value < 0.001, Fig. 9f). Finally, using inverse transformations to project our atlas into the space of each subject at each session, we found 40 regions, including the aforementioned cortices, whose overall volumes were significantly modified in the same direction (lower/greater volume) between winter and summer in sheep (Fig. 10 and Table S1).

4. Discussion

Using a new comprehensive neuroimaging resource dedicated to the sheep brain, this longitudinal study reveals the impact of the seasonal transition between winter and summer on the microstructural organization of the brain. Importantly, we observed significant variations of GMC in both the pineal gland and hypothalamus, two brain regions involved in circadian and circannual rhythms. Additionally, variations were noted within the thalamic suprageniculate nucleus, a major relay of the GHT that conveys light information from the periphery to the hypothalamic circadian pacemaker. These findings establish the validity of our MRI approach for studying seasonal microstructural modifications in the mammalian brain. Furthermore, we highlight significant modifications of GMC, GM thickness and regional volumes in numerous brain regions involved in various functions. Taken together, these results demonstrate the profound changes occurring between seasons in a seasonal mammal, suggesting that brain functioning switches between two *modus operandi* over the year.

4.1. *Implementation of novel resources to support the analysis of sheep brain MRI data*

Preclinical MRI is currently a hot topic (Homberg et al., 2021; Saito and Ueda, 2024; Wachsmuth et al., 2021), and the availability of population-average templates and well-defined brain atlases for animal models used in research represents a corner-stone for the development

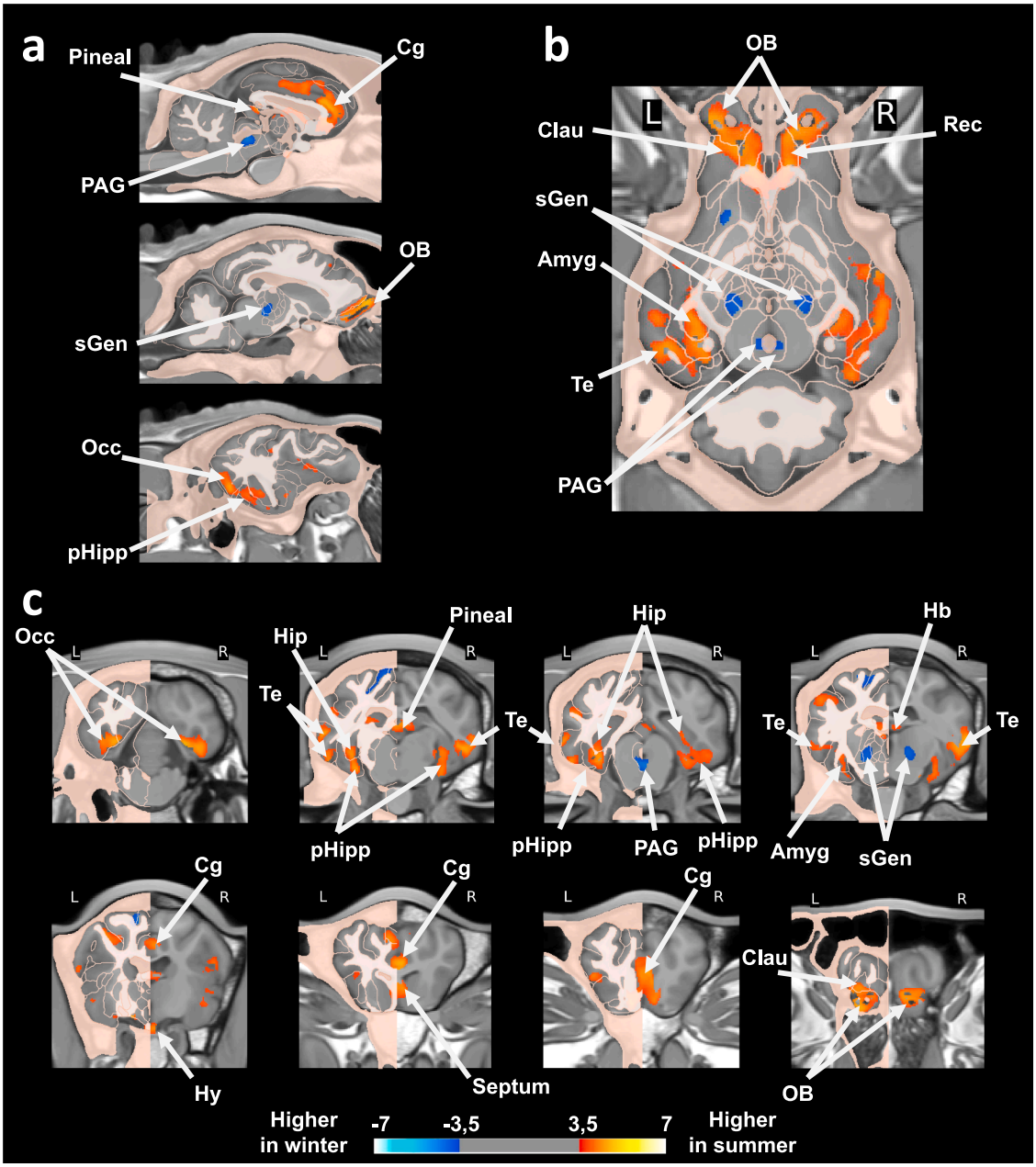

Fig. 4. Grey matter modifications induced by photoperiod (Winter < Summer). Sagittal (a) Coronal (b) and axial (c) slices showing grey matter concentration (GMC) differences between winter and summer.
SPM paired Student *t*-test analysis. Voxel-level threshold $p < 0.005$, $t_{(16)}=2.92$. *BNST=bed nucleus of the stria terminalis ; Hy=hypothalamus ; Hip=hippocampus ; pHipp=parahippocampal cortex ; PAG=periaqueductal grey substance ; Cg=cingulate cortex ; sGen=suprageniculate nucleus ; Occ=occipital gyrus ; Clau=claustrocortex (insula) ; Rec=rectus gyrus ; OB=olfactory bulb ; Pir=piriform cortex ; Amyg=amygdala ; Te=temporal gyrus; Hb=habenular nucleus.*

of preclinical imaging in neuroscience (Evans et al., 2012). Brain templates and atlases enable group studies and statistical analyses to investigate, for example, the size or volume of pivotal subcortical structures and GM thickness, based on anatomical imaging (T_1, T_2, T_{2*}). In the context of brain functional connectivity studies (fMRI), templates allow for spatial normalization of data and, through the definition of ROIs based on anatomically identified brain structures, to study modifications occurring within functional brain networks under different conditions (Barrière et al., 2019b). Also, recent progress in both diffusion and quantitative MRI allowed the development of multi-compartmental analytical models for signal analysis used to estimate the contribution of each cell population (neurons and glia) to the global signal (Zhang et al., 2012) or the estimation of the fraction of myelin (Kulikova et al., 2016) *in vivo*. Taken together, the multimodal ability of MRI is a powerful feature for studying the brain in health and disease, and its unique translatability between animal species broadens the horizons of the field. Multiple species, including pig, sheep, dogs and primates are still used in basic neurosciences andcould surpass rodents for the study of numerous conditions such as neuromuscular junction diseases (Cahalan et al., 2022), Batten disease (Jacobsen et al., 2022; Murray et al., 2023) but also for psychiatric conditions. Here, we used the ovine model to study the effect of the seasons on brain microstructural organisation as we ignore the inner mechanisms of the system that allows adaption of brain functioning and output behaviors to cope with seasonal changes. As marked seasons are associated with an increased prevalence of psychiatric conditions in humans, the study of brain modifications occurring in the sheep model is the first step to describe and study this adaptive system.

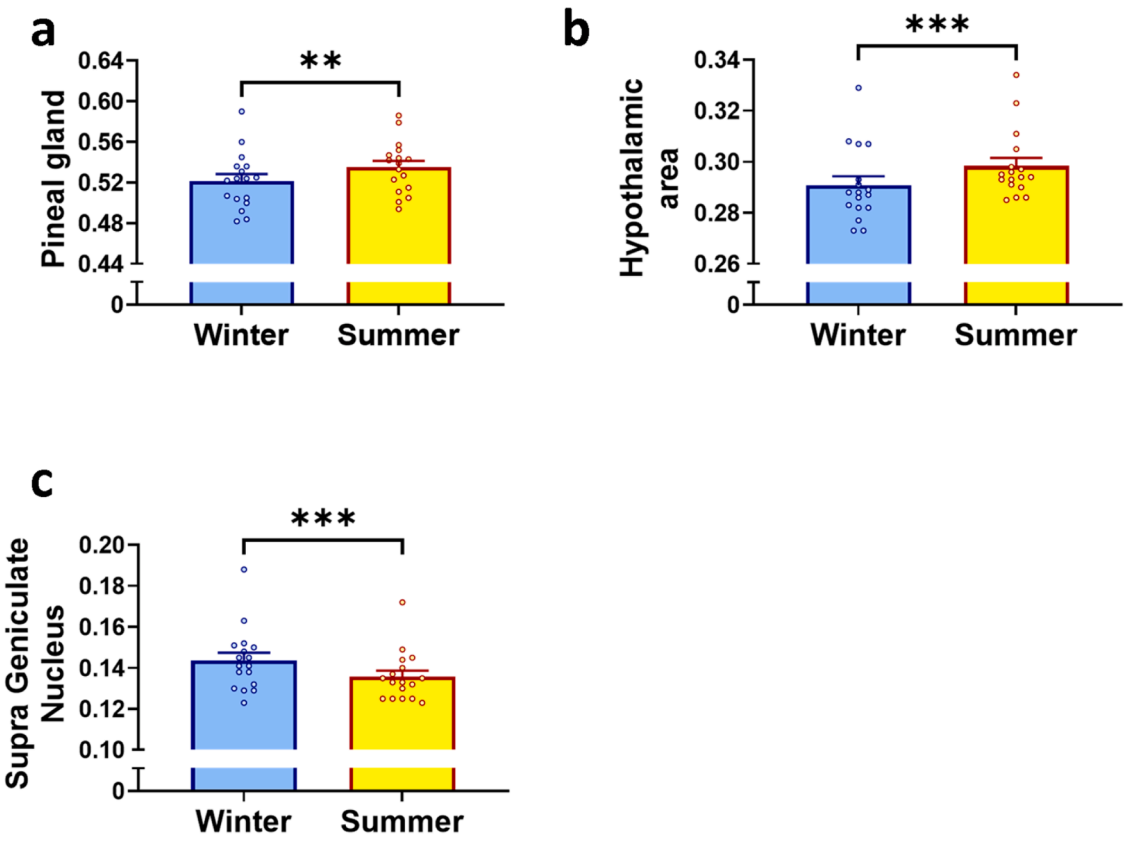

Fig. 5. Variations of grey matter concentration (GMC) over the seasons within main brain structures involved in the integration of light duration. Evolution of GMC between the winter (blue dots and box) and summer (yellow dots and box) in (a) pineal gland, (b) Hypothalamic area, (c) supragenicuiate nucleus of the thalamus. Data are expressed as the mean ± standard error of the mean (SEM); and compared using a Wilcoxon matched-pairs signed rank test using False Discovery Rate (FDR) for multiple comparisons and the two-stage step-up (Benjamini, Krieger and Yakutieli) method for a desired FDR (Q) value = 1 % (*** $p < 0.001$).

In the first part of our study, we generated a new set of neuroinformatics tools offering, for the first time, a complete resource dedicated to MRI studies of the ovine brain. This includes three high-resolution brain templates and their associated GM, WM and CSF priors with a resolution of 0.5 mm^3. The GM, WM, and CSF probabilistic maps built and used in this study were calculated from 34 anatomical images, resulting in robust tissue class priors for VBM analysis, as well as for functional MRI and diffusion tensor imaging analysis. We also provide an accurate sheep brain atlas composed of a mosaic of 208 ROI. This brain atlas offers an accurate segmentation of both cortical and subcortical areas, notably the thalamus, which had not yet been segmented in this species (Liyanage et al., 2016; Nitzsche et al., 2015). Additionally, we propose an additional CT template of the sheep skull, which allowed us to easily identify the lambda point used as a reference point to set the stereotaxic space. As the brain is oriented on the anterior commissure-posterior commissure (AC-PC) axis in our space and aligned alongside the interhemispheric sulcus, this spatial origin offers the possibility to navigate in three dimensions within the brain. These resources, available from the Zenodo website, will help conduct analyses of anatomical and functional datasets in a more standardized way.

4.2. Seasonal rythms in sheep

Using these resources and a VBM strategy, we identified significant modifications of the GMC in specific brain regions during the transition between winter (the breeding season) and summer (the non-breeding season). The exact nature of these GMC variations remains a topic of debate. These changes can be interpreted as alterations in cell size, neural or glial cell genesis or apoptosis, changes in spine density, or modifications in blood flow (Keifer et al., 2015; Lerch et al., 2011; Streitbürger et al., 2012). In a recent exploratory study that combined VBM measurements with *in vivo* two-photon imaging, the authors concluded that changes observed by VBM are not predominantly driven by changes in the actual volume of grey matter within a region (Asan et al., 2021). Instead, they proposed that local cell count, clustering characteristics of cells, and cell type composition are significant contributing factors to these modifications. This study also suggested the presence of region-specific processes (cortical *versus* subcortical), which may differentially influence GMC. These conclusions are in accordance with our results as we observed within the hypothalamus, significant modifications of GMC without modification of the GM thickness while major seasonal microstructural modifications involving neurogenesis, morphological modifications of tanycytes or microvascular rearrangements have been extensively described within the literature in this region (Chevillard et al., 2022; Migaud et al., 2015, 2011). Hence, to complete our VBM analysis, we measured the evolution over the seasons of both GM thickness and brain regional volumes. Together, these volumetric methodologies highlight regions like the parahippocampal and cingulate cortex, temporal gyrus, insula, amygdala, hippocampus, periaqueductal grey and olfactory tract/bulb where GM thickness and/or volume modifications are associated with modifications of the GMC. Interestingly, many other regions show significant modifications of thickness and/or volumes, which were not highlighted by the VBM approach, and vice versa. Furthers studies will be necessary to elucidate the links between GMC, GM thickness and regional volumes but in this context, the association of MRI with histological investigation in this seasonal animal model could be helpful for the biological characterization of these MRI metrics.

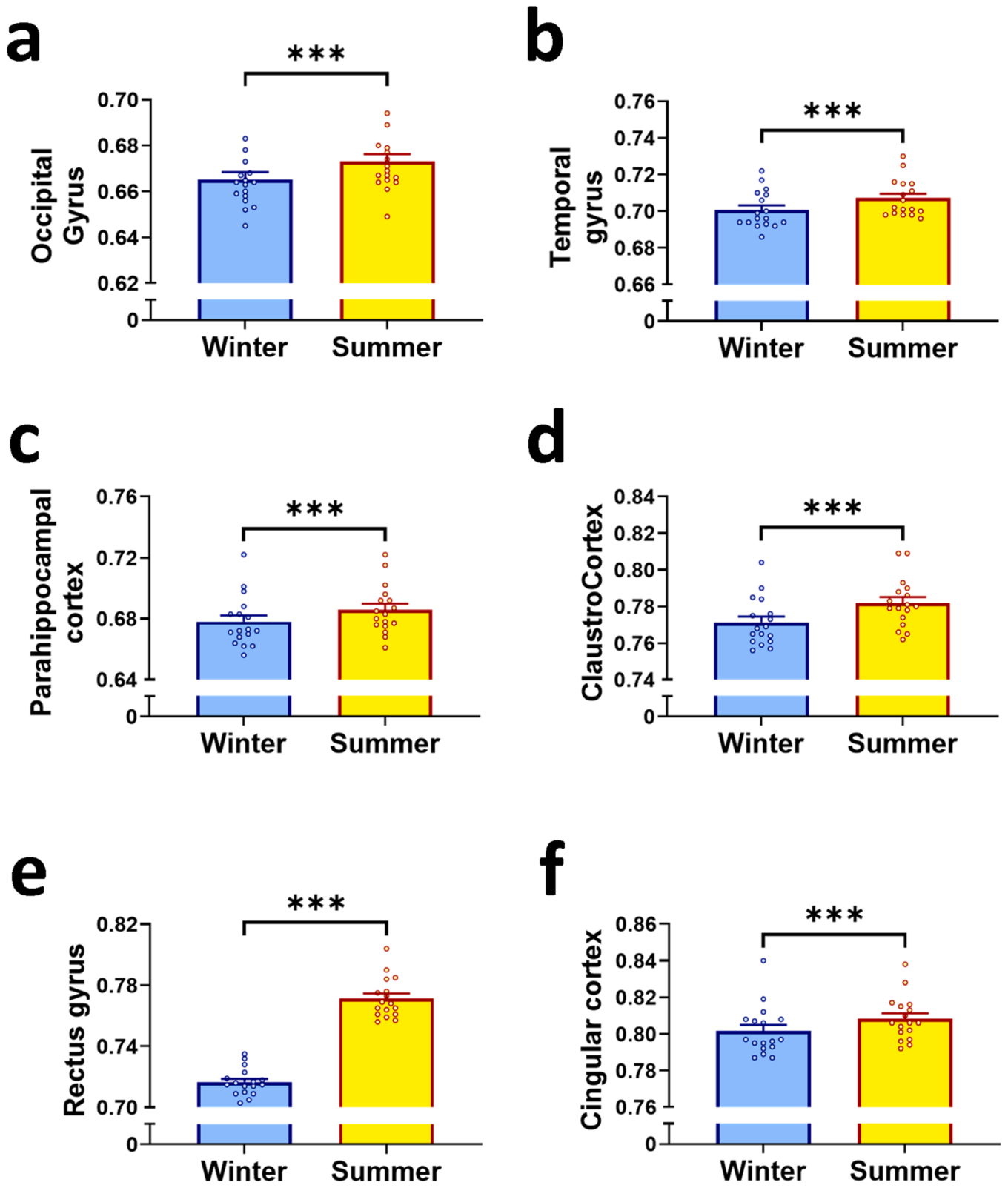

Fig. 6. Cortical variations of grey matter concentration (GMC) over the seasons. Evolution of the cortical GMC between the winter (blue dots and box) and summer (yellow dots and box) in (a) occipital gyrus, (b) temporal gyrus, (c) parahippocampal cortex, (d) claustrocortex (insula), (e) rectus gyrus, (f) cingulate cortex. Data are expressed as the mean ± standard error of the mean (SEM); and compared using a Wilcoxon matched-pairs signed rank test using False Discovery Rate (FDR) for multiple comparisons and the two-stage step-up (Benjamini, Krieger and Yakutieli) method for a desired FDR (Q) value = 1 % (*** $p < 0.001$).

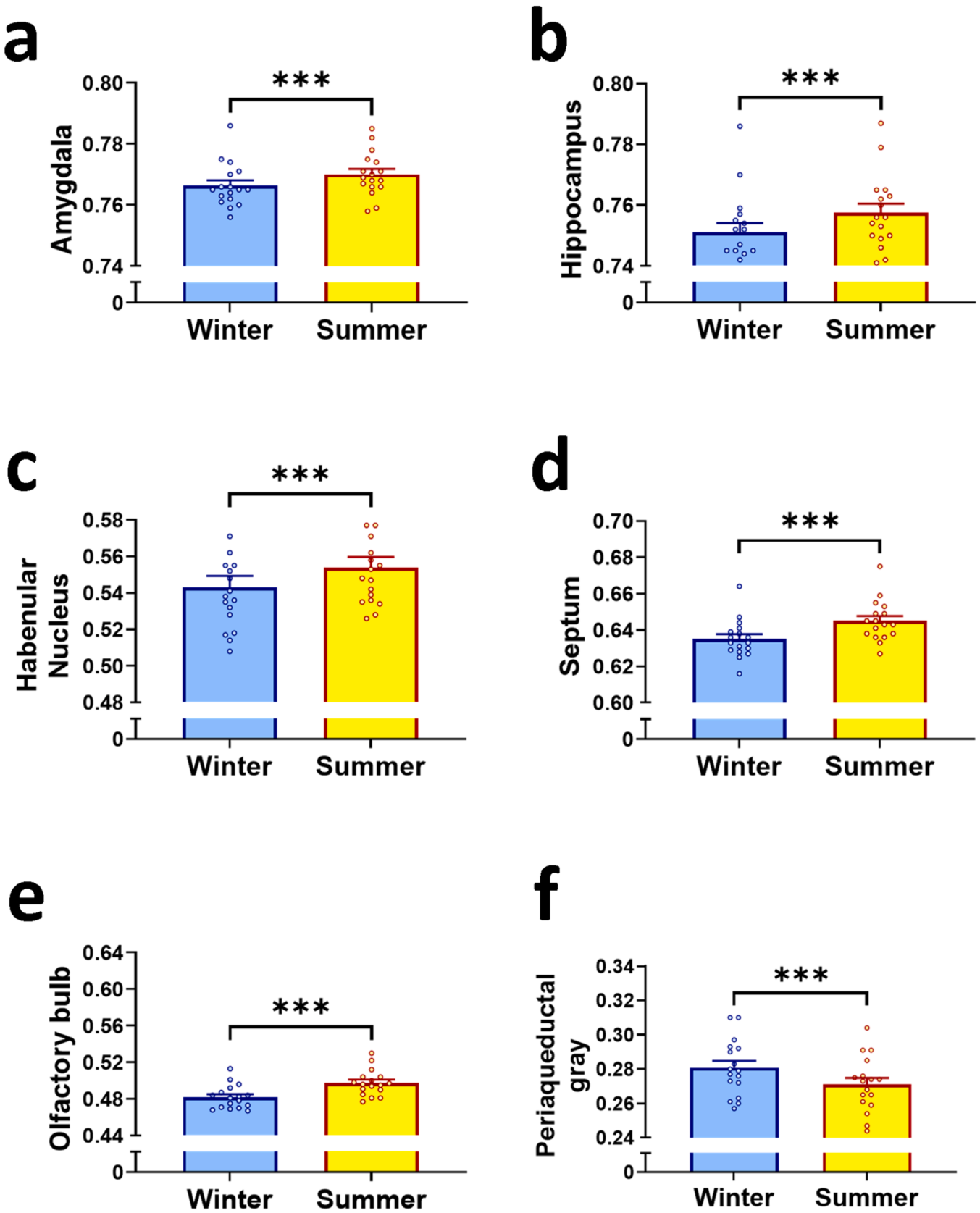

Fig. 7. Subcortical variations of grey matter concentration (GMC) over the seasons. Evolution of the subcortical GMC between the winter (blue dots and box) and summer (yellow dots and box) in (a) amygdala, (b) hippocampus, (c) habenular nucleus, (d) septum, (e) olfactory bulb, (f) periaqueductal grey substance. Data are expressed as the mean ± standard error of the mean (SEM); and compared using a Wilcoxon matched-pairs signed rank test using False Discovery Rate (FDR) for multiple comparisons and the two-stage step-up (Benjamini, Krieger and Yakutieli) method for a desired FDR (Q) value = 1 % (*** $p < 0.001$).

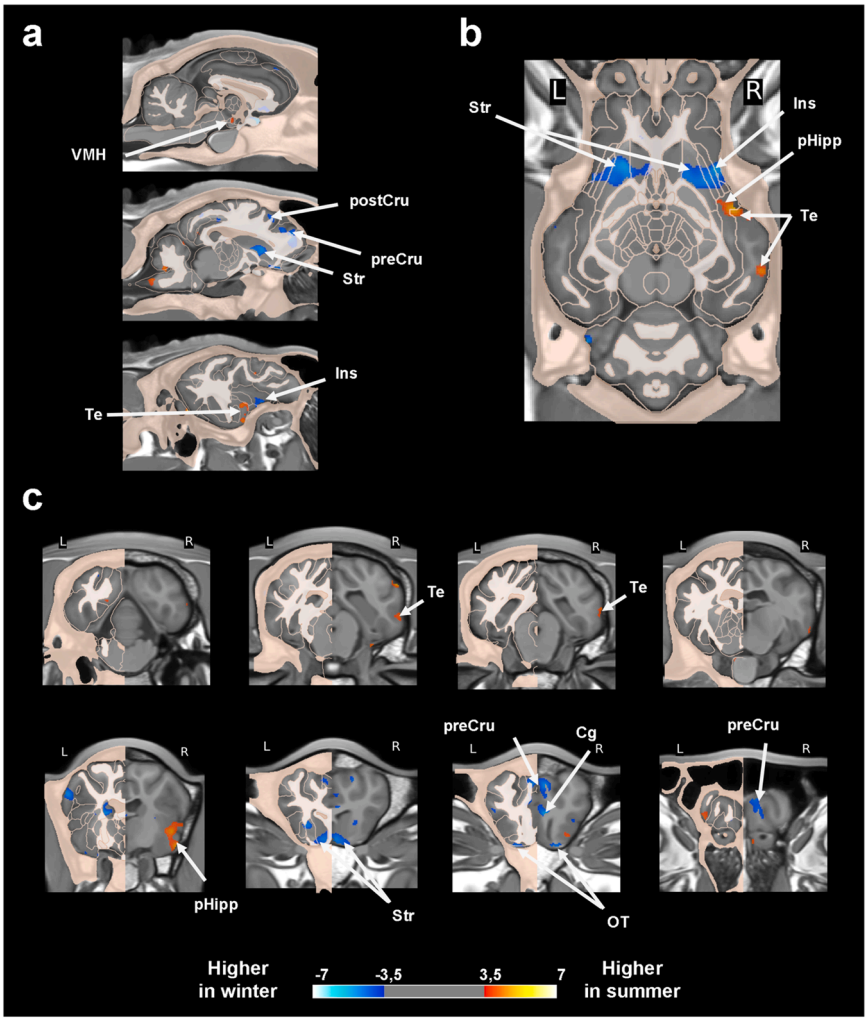

Fig. 8. GM thickness modifications induced by photoperiod (Winter < Summer). Sagittal (a) Coronal (b) and axial (c) slices showing grey matter concentration (GMC) differences between winter and summer.
SPM paired Student *t*-test analysis. Voxel-level threshold $p < 0.005$, $t_{(16)}=2.92$. *Cg=cingulate cortex ; Ins=insula ; pHipp=parahippocampal cortex ; preCru=precruciate gyrus ; postCru=postcruciate gyrus ; str=striatum ; Te=temporal gyrus; OT=olfactory tract ; VMH=Ventromedian hypothalamic nucleus.*

4.2.1. *Sheep physiology and behaviors over the seasons*

Seasons have a profound impact on sheep physiology and behavioural strategies, which adapt in response to environmental changes. Firstly, sheep undergo significant metabolic variations throughout the year. Their basal metabolic rate and food consumption follow a seasonal pattern, reaching the lowest levels in midwinter and peaking in midsummer, in accordance with food availability (Arnold and Pahl, 1974; Baldock et al., 1988). Consequently, feeding behaviors such as grazing, ruminating, and food seeking are more intense during the peak of food availability period in midsummer under natural conditions. Secondly, social behaviors are also influenced by seasonal changes. When food is scarce, animals may congregate to share information about food availability. Conversely, when food is abundant animals may spread out to maximize intake, thereby affecting social interactions (Freire et al., 2012). Lastly, the expression of sexual behaviors is finely tuned by seasonal changes. Photoperiodic signals regulate the activity of gonadotropin-releasing hormone (GnRH) neurons which ultimately control the steroid secretion by the gonads (Dardente et al., 2019; Migaud et al., 2015, 2011). In our recent MRI study on sheep, we revealed that sex hormones, in turn, profoundly reorganize the brain's microstructural and functional organization (Barrière et al., 2019a). This reorganization ultimately controls the expression of sociosexual behaviors such as calls, approach, aggression, territoriality, and acceptance. Taken together, both physiological and behavioural modifications imposed by seasonal changes engage numerous brain systems in different operative modes promoting the expression of behaviors and physiological modification that are suited to the varying conditions over the course of the seasons.

4.2.2. *Sheep brain over the seasons*

Our comprehensive, unbiased whole-brain MRI approach reveals structural plasticity in key brain regions whose involvement in seasonal functions, or at least their morphological sensitivity to seasonal changes, had not, to our knowledge, been previously documented in this model. Specifically, we observed significant seasonal modifications in GMC, GM thickness, and regional volume across brain systems associated with distinct functional domains. In sensory and integrative networks, alterations in the occipital gyrus (Pirone et al., 2021), temporal gyrus (Peirce and Kendrick, 2002), and parahippocampal cortex (Burwell, 2000) suggest adaptive adjustments in visual processing, multisensory integration, and spatial orientation, likely reflecting environmental demands. Within the learning and memory system, morphological changes in the hippocampus and cingulate cortex, alongside limbic structures such as the amygdala, habenular nucleus, and septum, indicate seasonal recalibration of cognitive flexibility, emotional regulation, and memory encoding. These modifications may underlie behavioural adaptations to

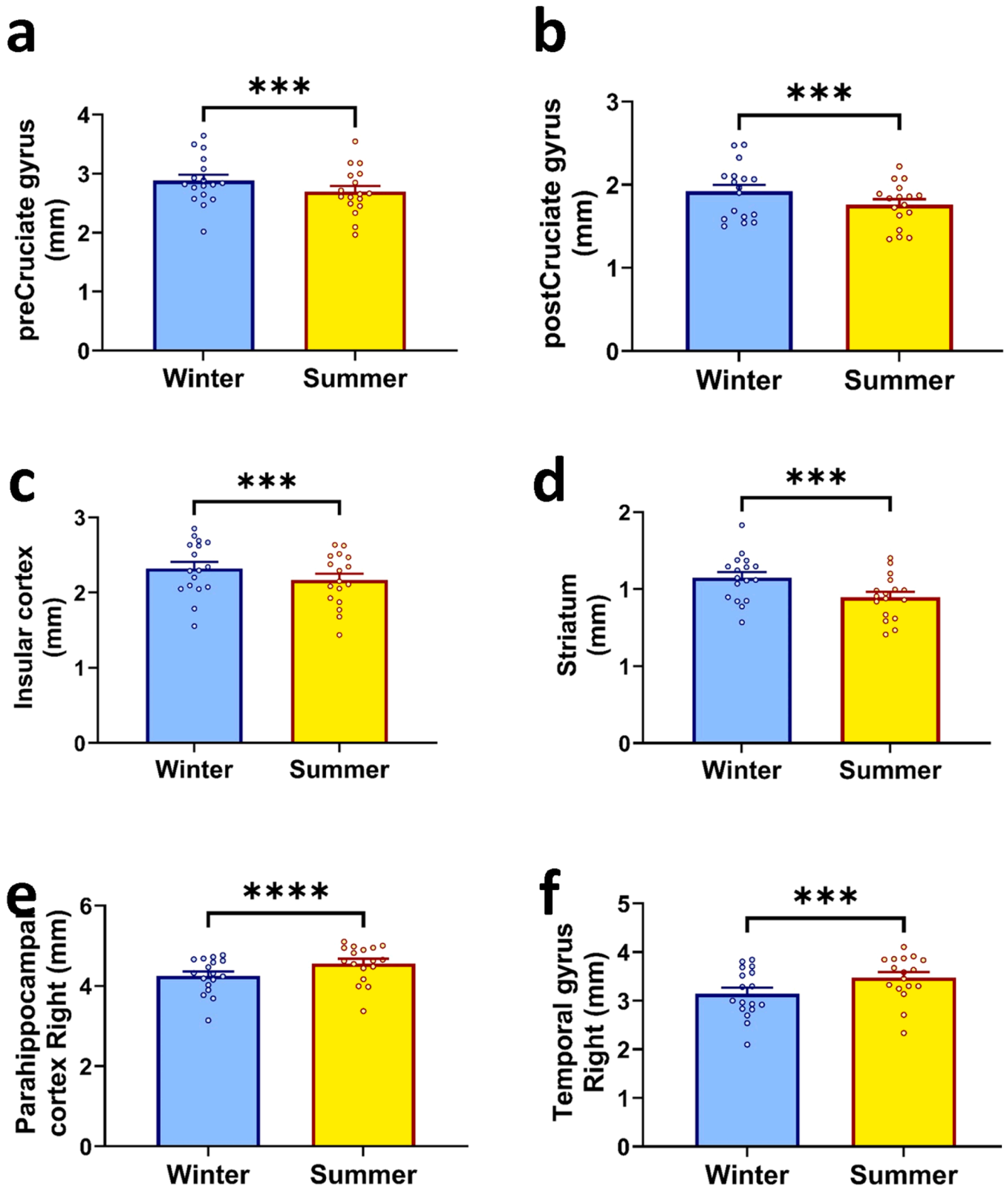

Fig. 9. GM thickness variations over the seasons. Evolution of the GM thickness between the winter (blue dots and box) and summer (yellow dots and box) in (a) precruciate gyrus, (b) postcruciate gyrus, (c) insular cortex and (d) striatum, (e) parahippocampal cortex, (f), Temporal gyrus.
Data are expressed as the mean ± standard error of the mean (SEM); and compared using a Wilcoxon matched-pairs signed rank test using False Discovery Rate (FDR) for multiple comparisons and the two-stage step-up (Benjamini, Krieger and Yakutieli) method for a desired FDR (Q) value = 1 % (*** $p < 0.001$).

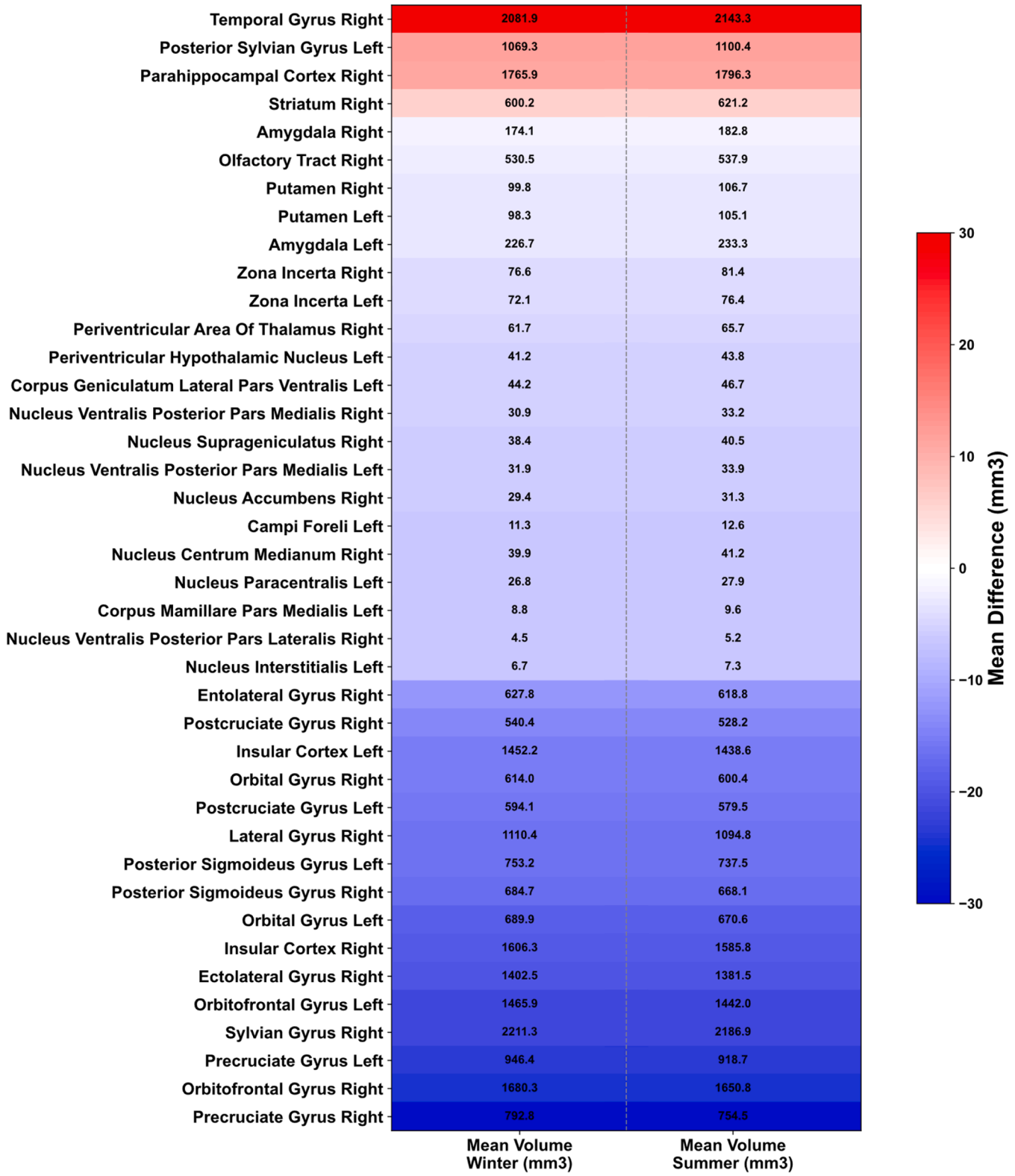

Fig. 10. Mean volume difference (in mm^3) between Summer and Winter. ROIs (region of interest) are sorted in descending order of difference, with positive values indicating an increase in volume between winter and summer periods, and negative values indicating a decrease. Colour gradient highlights the magnitude and direction of these seasonal changes. Only ROIs with a significant seasonal effect are included.
Significant ROIs have been identified by a linear regression model with fixed effects for subject and session, followed by a permutation-based correction (10.000 permutations) for multiple comparisons ($p < 0.05$).

shifting social or ecological contexts.

Notably, we also detected plasticity in the PAG, a critical node for defensive behaviors, reproduction, and maternal behaviors (Carrive, 1993; Van der Horst and Holstege, 1998; Wallin et al., 2021) functions known to exhibit seasonal variability in sheep, though their structural correlates had not been characterized until now. Further regions supporting a broad seasonal influence, the neurogenic regions, including the hypothalamus, olfactory bulb, and hippocampus (Batailler et al., 2018; Dardente et al., 2019; Migaud et al., 2015), displayed morphological changes, reinforcing the idea that seasonal cues drive cellular remodelling in areas governing homeostasis, olfaction, and episodic memory.

Together, these findings demonstrate that seasonality impacts not only classical reproductive or metabolic pathways but also higher-order cognitive and mnesic circuits. While the biological significance of this plasticity remains to be elucidated, our results challenge the traditional view of seasonal brain changes as restricted to hypothalamic or neuroendocrine systems. Instead, they point to a global, systems-level reorganization that may optimize behavior in response to cyclical environmental challenges.

4.2.3. Limitations

While this study advances our understanding of seasonal brain plasticity, several limitations must be considered when interpreting the results. First, although VBM is a standardized and widely used technique, the resulting GMC index is a non-specific metric that reflects multiple underlying processes, including changes in cell density, neurogenesis, gliosis, synaptic pruning, or vascularization. These processes likely contribute differently in a region-specific manner (e.g., cortical *versus* subcortical regions), adding another layer of complexity to the interpretation of GMC modifications. Second, the MPRAGE sequence used in this study provides only T_1-weighted contrast, not quantitative T_1 values. Consequently, observed GMC differences may be influenced by technical factors (e.g., coil inhomogeneities, scanner drift), which could account for inconsistencies between GMC, GM thickness, and volumetric measurements. In future studies, parametric quantitative MRI (qMRI) techniques, which provide physically meaningful metrics linked to tissue composition, will be required to accurately assess the effects of seasonal changes on brain parenchyma organization. Pairing this qMRI approach with high-resolution histology (e.g., immunohistochemistry for neuronal/glial markers, electron microscopy for synaptic density) would help clarify the biological significance of GMC fluctuations over the seasons.

5. Conclusions

By updating the TSBTA resources to meet human MR imaging standards, we demonstrated for the first time that seasonal photoperiodic shifts induce widespread and complex structural reorganization across the sheep brain. Through VBM, GM thickness analysis, and volumetric assessments we developed methods to study brain morphology in the ovine model. We revealed that the transition between winter and summer alters not only hypothalamic and pineal regions, but also cortical and limbic areas known to be involved in higher-order brain functions. The discovery of structural seasonal plasticity in non-hypothalamic regions raises new questions about the functional significance of these changes and their potential relevance to human seasonal affective disorders. Future studies integrating histology, functional imaging, and behavioural assays will be critical to unravel the cellular mechanisms driving these adaptations and their cognitive and emotional consequences. Ultimately, this research provides both a methodological framework for exploring how environmental rhythms shape the mammalian brain and a foundation for deeper investigations into adaptive and maladaptive responses to seasonal change.

Data availability

All data and code used and created in the present publication are freely available. Raw data: https://zenodo.org/records/11027441; templates, priors and atlas: https://zenodo.org/records/10730961 and codes: https://github.com/DavidBarriere/Photoperidic_Brain

CRediT authorship contribution statement

Arsène Ella: Methodology, Conceptualization. **Didier Chesneau:** Methodology. **Chantal Porte:** Methodology. **Didier Lomet:** Methodology. **Hans Adriaensen:** Methodology. **Benoit Piégu:** Methodology. **Ivy Uszynski:** Methodology. **Cyril Poupon:** Software, Resources, Methodology. **Martine Migaud:** Writing – review & editing, Conceptualization. **José Delgadillo:** Writing – review & editing, Conceptualization. **Tiphaine Aguirre-Lavin:** Resources. **Olivier Lasserre:** Resources, Methodology. **Philippe Chemineau:** Writing – review & editing, Methodology, Conceptualization. **Hugues Dardente:** Writing – review & editing, Validation, Supervision, Methodology, Investigation, Conceptualization. **Matthieu Keller:** Writing – review & editing, Validation, Supervision, Project administration, Methodology, Investigation, Funding acquisition, Formal analysis, Conceptualization. **David André Barrière:** Writing – review & editing, Writing – original draft, Visualization, Validation, Software, Resources, Project administration, Formal analysis, Data curation.

Declaration of competing interest

The authors declare that they have no known competing financial interests or personal relationships that could have appeared to influence the work reported in this paper.

Acknowledgments

This work was supported by French National Research Agency (ANR) grant MALE-EFFECT (ANR11-ISV7–0001, 2011–2015) to Matthieu Keller. This work was also supported by the French National Research Institute for Agriculture, Food and the Environment (INRAE), which, through its specific experimental units Unité Expérimentale de Physiologie Animale de l'Orfrasière (UEPAO), the PIXANIM imaging platform belonging to the UMR Physiologie de la Reproduction & des Comportements, provided both animals and technical facilities for successful MR imaging on domestic sheep. We are also grateful to Gilles Gomot and all the staff of the PIXANIM facility for ensuring that surgeries and monitoring of the animals during MRI scans were performed under optimal conditions from both experimental and animal welfare aspects. We would like to thank Damien Capo, Olivier Lasserre and all the shepherds for providing care to the animals.

This publication is dedicated to the memory of our colleague and friend Arsène Ella, who sadly passed away on February 14th, 2022. Arsène had a PhD in biomedical engineering with a great expertise in medical image processing. He started his career by characterizing the human myocardium in SPECT and positron emission tomography (PET) imaging using the thin-plate spline warping. He moved on to the analysis of the human brain through investigation of fDOPA kinetics and brain compartments in PET. Then, he implemented a new technique for correction of physiological noises in functional magnetic resonance imaging (fMRI). In collaboration with Matthieu Keller, Arsène developed the first complete 3D high-resolution probabilistic template and atlas of the sheep brain from MR images. The work reported here started in 2014, after publication of these key achievements (Ella et al., 2017; Ella and Keller, 2015). Pandemic breakthroughs and personal issues postponed publication for several years until Arsene sadly passed away. David A. Barrière took all the raw data and reanalysed them thoroughly. Posthumous Responsibilities of the authors: Matthieu Keller who granted the project and David A. Barriere who performed the final analysis

ensured together paper writing, editing and publishing and assume the authorship roles and responsibilities of the results and conclusions of the present paper.

Supplementary materials

Supplementary material associated with this article can be found, in the online version, at doi:10.1016/j.neuroimage.2025.121494.

References

Arnold, G.W., Pahl, P.J., 1974. Some aspects of social behaviour in domestic sheep. Anim. Behav. 22, 592–600. https://doi.org/10.1016/S0003-3472(74)80004-7.

Asan, L., Falfán-Melgoza, C., Beretta, C.A., Sack, M., Zheng, L., Weber-Fahr, W., Kuner, T., Knabbe, J., 2021. Cellular correlates of gray matter volume changes in magnetic resonance morphometry identified by two-photon microscopy. Sci. Rep. 11, 4234. https://doi.org/10.1038/s41598-021-83491-8.

Ashburner, J., 2007. A fast diffeomorphic image registration algorithm. Neuroimage 38, 95–113. https://doi.org/10.1016/j.neuroimage.2007.07.007.

Ashburner, J., Friston, K.J., 2005. Unified segmentation. Neuroimage 26, 839–851. https://doi.org/10.1016/j.neuroimage.2005.02.018.

Ashburner, J., Friston, K.J., 2000. Voxel-based morphometry–the methods. Neuroimage 11, 805–821. https://doi.org/10.1006/nimg.2000.0582.

Baldock, N.M., Sibly, R.M., Penning, P.D., 1988. Behaviour and seasonal variation in heart rate in domestic sheep, *Ovis aries*. Anim. Behav. 36, 35–43. https://doi.org/10.1016/S0003-3472(88)80247-1.

Barrière, David André, Ella, A., Adriaensen, H., Roselli, C.E., Chemineau, P., Keller, M., 2019a. In vivo magnetic resonance imaging reveals the effect of gonadal hormones on morphological and functional brain sexual dimorphisms in adult sheep. Psychoneuroendocrinology 109, 104387. https://doi.org/10.1016/j.psyneuen.2019.104387.

Barrière, D.A., Ella, A., Szeremeta, F., Adriaensen, H., Même, W., Chaillou, E., Migaud, M., Même, S., Lévy, F., Keller, M., 2021. Brain orchestration of pregnancy and maternal behavior in mice: a longitudinal morphometric study. Neuroimage 230, 117776. https://doi.org/10.1016/j.neuroimage.2021.117776.

Barrière, David André, Hamieh, A.M., Magalhães, R., Traoré, A., Barbier, J., Bonny, J.-M., Ardid, D., Busserolles, J., Mériaux, S., Marchand, F., 2019b. Structural and functional alterations in the retrosplenial cortex following neuropathic pain. Pain. https://doi.org/10.1097/j.pain.0000000000001610.

Barrière, D.A., Magalhães, R., Novais, A., Marques, P., Selingue, E., Geffroy, F., Marques, F., Cerqueira, J., Sousa, J.C., Boumezbeur, F., Bottlaender, M., Jay, T.M., Cachia, A., Sousa, N., Mériaux, S., 2019. The SIGMA rat brain templates and atlases for multimodal MRI data analysis and visualization. Nat. Commun. 10, 5699. https://doi.org/10.1038/s41467-019-13575-7.

Batailler, M., Chesneau, D., Derouet, L., Butruille, L., Segura, S., Cognié, J., Dupont, J., Pillon, D., Migaud, M., 2018. Pineal-dependent increase of hypothalamic neurogenesis contributes to the timing of seasonal reproduction in sheep. Sci. Rep. 8, 6188. https://doi.org/10.1038/s41598-018-24381-4.

Bauer, M., Glenn, T., Alda, M., Andreassen, O.A., Angelopoulos, E., Ardau, R., Ayhan, Y., Baethge, C., Bauer, R., Baune, B.T., Becerra-Palars, C., Bellivier, F., Belmaker, R.H., Berk, M., Bersudsky, Y., Bicakci, Ş., Birabwa-Oketcho, H., Bjella, T.D., Cabrera, J., Wo Cheung, E.Y., Del Zompo, M., Dodd, S., Donix, M., Etain, B., Fagiolini, A., Fountoulakis, K.N., Frye, M.A., Gonzalez-Pinto, A., Gottlieb, J.F., Grof, P., Harima, H., Henry, C., Isometsä, E.T., Janno, S., Kapczinski, F., Kardell, M., Khaldi, S., Kliwicki, S., König, B., Kot, T.L., Krogh, R., Kunz, M., Lafer, B., Landén, M., Larsen, E.R., Lewitzka, U., Licht, R.W., Lopez-Jaramillo, C., MacQueen, G., Manchia, M., Marsh, W., Martinez-Cengotitabengoa, M., Melle, I., Meza-Urzúa, F., Ming, M.Y., Monteith, S., Morken, G., Mosca, E., Mozzhegorov, A.A., Munoz, R., Mythri, S.V., Nacef, F., Nadella, R.K., Nery, F.G., Nielsen, R.E., O'Donovan, C., Omrani, A., Osher, Y., Sørensen, H.Ø., Ouali, U., Ruiz, Y.P., Pilhatsch, M., Pinna, M., da Ponte, F.D.R., Quiroz, D., Ramesar, R., Rasgon, N., Reddy, M.S., Reif, A., Ritter, P., Rybakowski, J.K., Sagduyu, K., Raghuraman, B.S., Scippa, Â.M., Severus, E., Simhandl, C., Stackhouse, P.W., Stein, D.J., Strejilevich, S., Subramaniam, M., Sulaiman, A.H., Suominen, K., Tagata, H., Tatebayashi, Y., Tondo, L., Torrent, C., Vaaler, A.E., Vares, E., Veeh, J., Vieta, E., Viswanath, B., Yoldi-Negrete, M., Zetin, M., Zgueb, Y., Whybrow, P.C., 2019. Association between solar insolation and a history of suicide attempts in bipolar I disorder. J. Psychiatr. Res. 113, 1–9. https://doi.org/10.1016/j.jpsychires.2019.03.001.

Burwell, R.D., 2000. The parahippocampal region: corticocortical connectivity. Ann. N. Y. Acad. Sci. 911, 25–42. https://doi.org/10.1111/j.1749-6632.2000.tb06717.x.

Cahalan, S.D., Boehm, I., Jones, R.A., Piercy, R.J., 2022. Recognising the potential of large animals for modelling neuromuscular junction physiology and disease. J. Anat. 241, 1120–1132. https://doi.org/10.1111/joa.13749.

Carrive, P., 1993. The periaqueductal gray and defensive behavior: functional representation and neuronal organization. Behav. Brain Res. 58, 27–47. https://doi.org/10.1016/0166-4328(93)90088-8.

Chevillard, P.-M., Batailler, M., Piégu, B., Estienne, A., Blache, M.-C., Dubois, J.-P., Pillon, D., Vaudin, P., Dupont, J., Just, N., Migaud, M., 2022. Seasonal vascular plasticity in the mediobasal hypothalamus of the adult ewe. Histochem. Cell Biol. 157, 581–593. https://doi.org/10.1007/s00418-022-02079-z.

Dardente, H., 2015. Circannual biology: the double life of the seasonal thyrotroph. Curr. Biol. 25, R988–R991. https://doi.org/10.1016/j.cub.2015.09.002.

Dardente, H., Hazlerigg, D.G., Ebling, F.J.P., 2014. Thyroid hormone and seasonal rhythmicity. Front. Endocrinol. (Lausanne) 5, 19. https://doi.org/10.3389/fendo.2014.00019.

Dardente, H., Wood, S., Ebling, F., Sáenz de Miera, C., 2019. An integrative view of mammalian seasonal neuroendocrinology. J. Neuroendocrinol. 31, e12729. https://doi.org/10.1111/jne.12729.

Das, S.R., Avants, B.B., Grossman, M., Gee, J.C., 2009. Registration based cortical thickness measurement. Neuroimage 45, 867–879. https://doi.org/10.1016/j.neuroimage.2008.12.016.

Desrosiers-Grégoire, G., Devenyi, G.A., Grandjean, J., Chakravarty, M.M., 2024. A standardized image processing and data quality platform for rodent fMRI. Nat. Commun. 15, 6708. https://doi.org/10.1038/s41467-024-50826-8.

Ella, A., Delgadillo, J.A., Chemineau, P., Keller, M., 2017. Computation of a high-resolution MRI 3D stereotaxic atlas of the sheep brain. J. Comp. Neurol. 525, 676–692. https://doi.org/10.1002/cne.24079.

Ella, A., Keller, M., 2015. Construction of an MRI 3D high resolution sheep brain template. Magn. Reson. ImAging 33, 1329–1337. https://doi.org/10.1016/j.mri.2015.09.001.

Evans, A.C., Janke, A.L., Collins, D.L., Baillet, S., 2012. Brain templates and atlases. Neuroimage 62, 911–922. https://doi.org/10.1016/j.neuroimage.2012.01.024.

Fraser, S., Cowen, P., Franklin, M., Franey, C., Arendt, J., 1983. Direct radioimmunoassay for melatonin in plasma. Clin. Chem. 29, 396–397.

Freire, R., Swain, D.L., Friend, M.A., 2012. Spatial distribution patterns of sheep following manipulation of feeding motivation and food availability. Animal 6, 846–851. https://doi.org/10.1017/S1751731111002126.

Grandjean, J., Desrosiers-Gregoire, G., Anckaerts, C., Angeles-Valdez, D., Ayad, F., Barrière, D.A., Blockx, I., Bortel, A., Broadwater, M., Cardoso, B.M., Célestine, M., Chavez-Negrete, J.E., Choi, S., Christiaen, E., Clavijo, P., Colon-Perez, L., Cramer, S., Daniele, T., Dempsey, E., Diao, Y., Doelemeyer, A., Dopfel, D., Dvořáková, L., Falfán-Melgoza, C., Fernandes, F.F., Fowler, C.F., Fuentes-Ibañez, A., Garin, C.M., Gelderman, E., Golden, C.E.M., Guo, C.C.G., Henckens, M.J.A.G., Hennessy, L.A., Herman, P., Hofwijks, N., Horien, C., Ionescu, T.M., Jones, J., Kaesser, J., Kim, E., Lambers, H., Lazari, A., Lee, S.-H., Lillywhite, A., Liu, Y., Liu, Y.Y., López-Castro, A., López-Gil, X., Ma, Z., MacNicol, E., Madularu, D., Mandino, F., Marciano, S., McAuslan, M.J., McCunn, P., McIntosh, A., Meng, X., Meyer-Baese, L., Missault, S., Moro, F., Naessens, D.M.P., Nava-Gomez, L.J., Nonaka, H., Ortiz, J.J., Paasonen, J., Peeters, L.M., Pereira, M., Perez, P.D., Pompilus, M., Prior, M., Rakhmatullin, R., Reimann, H.M., Reinwald, J., Del Rio, R.T., Rivera-Olvera, A., Ruiz-Pérez, D., Russo, G., Rutten, T.J., Ryoke, R., Sack, M., Salvan, P., Sanganahalli, B.G., Schroeter, A., Seewoo, B.J., Selingue, E., Seuwen, A., Shi, B., Sirmpilatze, N., Smith, J.A.B., Smith, C., Sobczak, F., Stenroos, P.J., Straathof, M., Strobelt, S., Sumiyoshi, A., Takahashi, K., Torres-García, M.E., Tudela, R., van den Berg, M., van der Marel, K., van Hout, A.T.B., Vertullo, R., Vidal, B., Vrooman, R.M., Wang, V.X., Wank, I., Watson, D.J.G., Yin, T., Zhang, Y., Zurbruegg, S., Achard, S., Alcauter, S., Auer, D.P., Barbier, E.L., Baudewig, J., Beckmann, C.F., Beckmann, N., Becq, G.J.P.C., Blezer, E.L.A., Bolbos, R., Boretius, S., Bouvard, S., Budinger, E., Buxbaum, J.D., Cash, D., Chapman, V., Chuang, K.-H., Ciobanu, L., Coolen, B.F., Dalley, J.W., Dhenain, M., Dijkhuizen, R.M., Esteban, O., Faber, C., Febo, M., Feindel, K.W., Forloni, G., Fouquet, J., Garza-Villarreal, E.A., Gass, N., Glennon, J.C., Gozzi, A., Gröhn, O., Harkin, A., Heerschap, A., Helluy, X., Herfert, K., Heuser, A., Homberg, J. R., Houwing, D.J., Hyder, F., Ielacqua, G.D., Jelescu, I.O., Johansen-Berg, H., Kaneko, G., Kawashima, R., Keilholz, S.D., Keliris, G.A., Kelly, C., Kerskens, C., Khokhar, J.Y., Kind, P.C., Langlois, J.-B., Lerch, J.P., López-Hidalgo, M.A., Manahan-Vaughan, D., Marchand, F., Mars, R.B., Marsella, G., Micotti, E., Muñoz-Moreno, E., Near, J., Niendorf, T., Otte, W.M., Pais-Roldán, P., Pan, W.-J., Prado-Alcalá, R.A., Quirarte, G.L., Rodger, J., Rosenow, T., Sampaio-Baptista, C., Sartorius, A., Sawiak, S.J., Scheenen, T.W.J., Shemesh, N., Shih, Y.-Y.I., Shmuel, A., Soria, G., Stoop, R., Thompson, G.J., Till, S.M., Todd, N., Van Der Linden, A., van der Toorn, A., van Tilborg, G.A.F., Vanhove, C., Veltien, A., Verhoye, M., Wachsmuth, L., Weber-Fahr, W., Wenk, P., Yu, X., Zerbi, V., Zhang, N., Zhang, B.B., Zimmer, L., Devenyi, G.A., Chakravarty, M.M., Hess, A., 2023. A consensus protocol for functional connectivity analysis in the rat brain. Nat. Neurosci. 26, 673–681. https://doi.org/10.1038/s41593-023-01286-8.

Hazlerigg, D., Simonneaux, V., 2015. Seasonal regulation of reproduction in mammals. Knobil and Neill's Physiology of Reproduction. Elsevier, pp. 1575–1604. https://doi.org/10.1016/B978-0-12-397175-3.00034-X.

Homberg, J.R., Adan, R.A.H., Alenina, N., Asiminas, A., Bader, M., Beckers, T., Begg, D. P., Blokland, A., Burger, M.E., van Dijk, G., Eisel, U.L.M., Elgersma, Y., Englitz, B., Fernandez-Ruiz, A., Fitzsimons, C.P., van Dam, A.-M., Gass, P., Grandjean, J., Havekes, R., Henckens, M.J.A.G., Herden, C., Hut, R.A., Jarrett, W., Jeffrey, K., Jezova, D., Kalsbeek, A., Kamermans, M., Kas, M.J., Kasri, N.N., Kiliaan, A.J., Kolk, S.M., Korosi, A., Korte, S.M., Kozicz, T., Kushner, S.A., Leech, K., Lesch, K.-P., Lesscher, H., Lucassen, P.J., Luthi, A., Ma, L., Mallien, A.S., Meerlo, P., Mejias, J.F., Meye, F.J., Mitchell, A.S., Mul, J.D., Olcese, U., González, A.O., Olivier, J.D.A., Pasqualetti, M., Pennartz, C.M.A., Popik, P., Prickaerts, J., de la Prida, L.M., Ribeiro, S., Roozendaal, B., Rossato, J.I., Salari, A.-A., Schoemaker, R.G., Smit, A.B., Vanderschuren, L.J.M.J., Takeuchi, T., van der Veen, R., Smidt, M.P., Vyazovskiy, V. V., Wiesmann, M., Wierenga, C.J., Williams, B., Willuhn, I., Wöhr, M., Wolvekamp, M., van der Zee, E.A., Genzel, L., 2021. The continued need for animals to advance brain research. Neuron 109, 2374–2379. https://doi.org/10.1016/j.neuron.2021.07.015.

Huang, L., Huang, T., Zhen, Z., Liu, J., 2016. A test-retest dataset for assessing long-term reliability of brain morphology and resting-state brain activity. Sci. Data 3, 160016. https://doi.org/10.1038/sdata.2016.16.

Iglesias, J.E., Insausti, R., Lerma-Usabiaga, G., Bocchetta, M., Van Leemput, K., Greve, D. N., van der Kouwe, A., Fischl, B., Caballero-Gaudes, C., Paz-Alonso, P.M., 2018.

A probabilistic atlas of the human thalamic nuclei combining ex vivo MRI and histology. Neuroimage 183, 314–326. https://doi.org/10.1016/j.neuroimage.2018.08.012.

Jacobsen, L., Daily, J., Murray, S., Palmer, D., Mitchell, N., Beausoleil, E., Albanis, E., 2022. Efficacy of gene therapy in a CLN5 sheep model using a dual route of administration supports a first-in-human clinical trial. Mol. Genet. Metab. 135, S62. https://doi.org/10.1016/j.ymgme.2021.11.154.

Karsch, F.J., Bittman, E.L., Foster, D.L., Goodman, R.L., Legan, S.J., Robinson, J.E., 1984. Neuroendocrine basis of seasonal reproduction. Recent. Prog. Horm. Res. 40, 185–232. https://doi.org/10.1016/b978-0-12-571140-1.50010-4.

Kegel, M., Dam, H., Ali, F., Bjerregaard, P., 2009. The prevalence of seasonal affective disorder (SAD) in Greenland is related to latitude. Nord. J. Psychiatry 63, 331–335. https://doi.org/10.1080/08039480902799040.

Keifer, O.P., Hurt, R.C., Gutman, D.A., Keilholz, S.D., Gourley, S.L., Ressler, K.J., 2015. Voxel-based morphometry predicts shifts in dendritic spine density and morphology with auditory fear conditioning. Nat. Commun. 6, 7582. https://doi.org/10.1038/ncomms8582.

Kinney, D.K., Teixeira, P., Hsu, D., Napoleon, S.C., Crowley, D.J., Miller, A., Hyman, W., Huang, E., 2009. Relation of schizophrenia prevalence to latitude, climate, fish consumption, infant mortality, and skin color: a role for prenatal vitamin d deficiency and infections? Schizophr. Bull. 35, 582–595. https://doi.org/10.1093/schbul/sbp023.

Kleven, H., Bjerke, I.E., Clascá, F., Groenewegen, H.J., Bjaalie, J.G., Leergaard, T.B., 2023. Waxholm space atlas of the rat brain: a 3D atlas supporting data analysis and integration. Nat. Methods 20, 1822–1829. https://doi.org/10.1038/s41592-023-02034-3.

Kulikova, S., Hertz-Pannier, L., Dehaene-Lambertz, G., Poupon, C., Dubois, J., 2016. A new strategy for fast MRI-based quantification of the myelin water fraction: application to brain imaging in infants. PLoS One 11, e0163143. https://doi.org/10.1371/journal.pone.0163143.

Legan, S.J., Karsch, F.J., Foster, D.L., 1977. The endocrin control of seasonal reproductive function in the ewe: a marked change in response to the negative feedback action of estradiol on luteinizing hormone secretion. Endocrinology 101, 818–824. https://doi.org/10.1210/endo-101-3-818.

Lerch, J.P., Yiu, A.P., Martinez-Canabal, A., Pekar, T., Bohbot, V.D., Frankland, P.W., Henkelman, R.M., Josselyn, S.A., Sled, J.G., 2011. Maze training in mice induces MRI-detectable brain shape changes specific to the type of learning. Neuroimage 54, 2086–2095. https://doi.org/10.1016/j.neuroimage.2010.09.086.

Liyanage, K.A., Steward, C., Moffat, B.A., Opie, N.L., Rind, G.S., John, S.E., Ronayne, S., May, C.N., O'Brien, T.J., Milne, M.E., Oxley, T.J., 2016. Development and implementation of a Corriedale Ovine brain atlas for use in atlas-based segmentation. PLoS One 11, e0155974. https://doi.org/10.1371/journal.pone.0155974.

Magnotta, V.A., Friedman, L., 2006. Measurement of signal-to-noise and contrast-to-noise in the fBIRN multicenter imaging study. J. Digit. Imaging 19, 140–147. https://doi.org/10.1007/s10278-006-0264-x.

Mandino, F., Cerri, D.H., Garin, C.M., Straathof, M., van Tilborg, G.A.F., Chakravarty, M. M., Dhenain, M., Dijkhuizen, R.M., Gozzi, A., Hess, A., Keilholz, S.D., Lerch, J.P., Shih, Y.-Y.I., Grandjean, J., 2020. Animal functional magnetic resonance imaging: trends and path toward standardization. Front. Neuroinform. 13. https://doi.org/10.3389/fninf.2019.00078.

Meyer, C., Muto, V., Jaspar, M., Kussé, C., Lambot, E., Chellappa, S.L., Degueldre, C., Balteau, E., Luxen, A., Middleton, B., Archer, S.N., Collette, F., Dijk, D.-J., Phillips, C., Maquet, P., Vandewalle, G., 2016. Seasonality in human cognitive brain responses. Proc. Natl. Acad. Sci. U.S.A. 113, 3066–3071. https://doi.org/10.1073/pnas.1518129113.

Migaud, M., Batailler, M., Pillon, D., Franceschini, I., Malpaux, B., 2011. Seasonal changes in cell proliferation in the adult sheep brain and pars tuberalis. J. Biol. Rhythms 26, 486–496. https://doi.org/10.1177/0748730411420062.

Migaud, M., Butrille, L., Batailler, M., 2015. Seasonal regulation of structural plasticity and neurogenesis in the adult mammalian brain: focus on the sheep hypothalamus. Front. Neuroendocrinol. 37, 146–157. https://doi.org/10.1016/j.yfrne.2014.11.004.

Murray, S.J., Almuqbel, M.M., Felton, S.A., Palmer, N.J., Myall, D.J., Shoorangiz, R., Ella, A., Keller, M., Palmer, D.N., Melzer, T.R., Mitchell, N.L., 2023. Progressive MRI brain volume changes in ovine models of CLN5 and CLN6 neuronal ceroid lipofuscinosis. Brain Commun. 5, fcac339. https://doi.org/10.1093/braincomms/fcac339.

Nitzsche, B., Frey, S., Collins, L.D., Seeger, J., Lobsien, D., Dreyer, A., Kirsten, H., Stoffel, M.H., Fonov, V.S., Boltze, J., 2015. A stereotaxic, population-averaged T1w ovine brain atlas including cerebral morphology and tissue volumes. Front. Neuroanat. 9, 69. https://doi.org/10.3389/fnana.2015.00069.

Patten, S.B., Williams, J.V.A., Lavorato, D.H., Wang, J.L., Bulloch, A.G.M., 2017. Major depression prevalence increases with latitude in Canada. Can. J. Psychiatry 62, 62–66. https://doi.org/10.1177/0706743716673323.

Peirce, J.W., Kendrick, K.M., 2002. Functional asymmetry in sheep temporal cortex. Neuroreport 13, 2395–2399. https://doi.org/10.1097/00001756-200212200-00004.

Pirone, A., Graïc, J., Grisan, E., Cozzi, B., 2021. The claustrum of the sheep and its connections to the visual cortex. J. Anat. 238, 1–12. https://doi.org/10.1111/joa.13302.

Ravault, J.-P., Arendt, J., Tobler, I., Chesneau, D., Maulin, O., 1989. Entrainment of melatonin rhythms in rams by symmetrical light-dark cycles of different period length. Chronobiol. Int. 6, 329–339. https://doi.org/10.3109/07420528909056939.

Rosen, L.N., Targum, S.D., Terman, M., Bryant, M.J., Hoffman, H., Kasper, S.F., Hamovit, J.R., Docherty, J.P., Welch, B., Rosenthal, N.E., 1990. Prevalence of seasonal affective disorder at four latitudes. Psychiatry Res. 31, 131–144. https://doi.org/10.1016/0165-1781(90)90116-m.

Saito, S., Ueda, J., 2024. Preclinical magnetic resonance imaging and spectroscopy in the fields of radiological technology, medical physics, and radiology. Radiol. Phys. Technol. 17, 47–59. https://doi.org/10.1007/s12194-024-00785-y.

Streitbürger, D.-P., Möller, H.E., Tittgemeyer, M., Hund-Georgiadis, M., Schroeter, M.L., Mueller, K., 2012. Investigating structural brain changes of dehydration using voxel-based morphometry. PLoS One 7, e44195. https://doi.org/10.1371/journal.pone.0044195.

Tillet, Y., Ravault, J.P., Selve, C., Evin, G., Castro, B., Dubois, M.P., 1986. Immunohistochemical visualization of serotonin and melatonin in the sheep pineal gland using specific antibodies. Comptes Rendus De L Academie Des Sciences Serie III 303.

Vakkuri, O., Leppäluoto, J., Vuolteenaho, O., 1984. Development and validation of a melatonin radioimmunoassay using radioiodinated melatonin as tracer. Acta Endocrinol. (Copenh) 106, 152–157. https://doi.org/10.1530/acta.0.1060152.

Van der Horst, V.G., Holstege, G., 1998. Sensory and motor components of reproductive behavior: pathways and plasticity. Behav. Brain Res. 92, 157–167. https://doi.org/10.1016/s0166-4328(97)00188-5.

Vrooman, R.M., van den Berg, M., Desrosiers-Gregoire, G., van Engelenburg, W.A., Galteau, M.E., Lee, S.-H., Veltien, A., Barrière, D.A., Cash, D., Chakravarty, M.M., Devenyi, G.A., Gozzi, A., Gröhn, O., Hess, A., Homberg, J.R., Jelescu, I.O., Keliris, G. A., Scheenen, T., Shih, Y.-Y.I., Verhoye, M., Wary, C., Zwiers, M., Grandjean, J., 2025. fMRI data acquisition and analysis for task-free, anesthetized rats. Nat. Protoc. 20, 1393–1412. https://doi.org/10.1038/s41596-024-01110-y.

Wachsmuth, L., Mensen, A., Barca, C., Wiart, M., Tristão-Pereira, C., Busato, A., Waiczies, S., Himmelreich, U., Millward, J.M., Reimann, H.M., Jelescu, I., Marzola, P., Pradier, B., Viola, A., Faber, C., 2021. Contribution of preclinical MRI to responsible animal research: living up to the 3R principle. MAGMa 34, 469–474. https://doi.org/10.1007/s10334-021-00929-w.

Wallin, C.M., Bowen, S.E., Brummelte, S., 2021. Opioid use during pregnancy can impair maternal behavior and the maternal brain network: a literature review. Neurotoxicol. Teratol. 86, 106976. https://doi.org/10.1016/j.ntt.2021.106976.

Wang, Q., Ding, S.-L., Li, Y., Royall, J., Feng, D., Lesnar, P., Graddis, N., Naeemi, M., Facer, B., Ho, A., Dolbeare, T., Blanchard, B., Dee, N., Wakeman, W., Hirokawa, K.E., Szafer, A., Sunkin, S.M., Oh, S.W., Bernard, A., Phillips, J.W., Hawrylycz, M., Koch, C., Zeng, H., Harris, J.A., Ng, L., 2020. The Allen mouse brain common coordinate framework: a 3D reference atlas. Cell 181, 936–953. https://doi.org/10.1016/j.cell.2020.04.007 e20.

Webley, G.E., Luck, M.R., 1986. Melatonin directly stimulates the secretion of progesterone by human and bovine granulosa cells in vitro. Reproduction 78, 711–717. https://doi.org/10.1530/jrf.0.0780711.

Xu, L., Choi, S., Zhao, Y., Li, M., Rogers, B.P., Anderson, A., Gore, J.C., Gao, Y., Ding, Z., 2023. Seasonal variations of functional connectivity of human brains. Sci. Rep. 13, 16898. https://doi.org/10.1038/s41598-023-43152-4.

Zarazaga, L.A., Celi, I., Guzmán, J.L., Malpaux, B., 2010. Melatonin concentrations in the two jugular veins, and relationship with the seasonal reproductive activity in goats. Theriogenology 74, 221–228. https://doi.org/10.1016/j.theriogenology.2010.02.005.

Zhang, H., Schneider, T., Wheeler-Kingshott, C.A., Alexander, D.C., 2012. NODDI: practical in vivo neurite orientation dispersion and density imaging of the human brain. Neuroimage 61, 1000–1016. https://doi.org/10.1016/j.neuroimage.2012.03.072.

Zhang, R., Shokri-Kojori, E., Volkow, N.D., 2023. Seasonal effect—An overlooked factor in neuroimaging research. Transl. Psychiatry 13, 238. https://doi.org/10.1038/s41398-023-02530-2.

Zhang, R., Volkow, N.D., 2023. Seasonality of brain function: role in psychiatric disorders. Transl. Psychiatry 13, 1–11. https://doi.org/10.1038/s41398-023-02365-x.